Oxygen Scavengers in Polyethylene Terephthalate (PET) for Recycled Food Packaging

HAFSA BAHADAR

Oxygen Scavengers in Polyethylene Terephthalate (PET) for Recycled Food Packaging

HAFSA BAHADAR

A thesis submitted in fulfilment of the degree of Master of Science by Research (MSc) at Manchester Metropolitan University

Department of Natural Sciences

Manchester Metropolitan University

In collaboration with

Avient Material Solutions UK Ltd.

Abstract

The oxidation of diene esters, which mimic the properties of Amosorb®, was investigated to understand the oxidation chemistry of Amosorb®. Model compounds — trans-2,4-hexadienyl acetate (1) and trans-2,4-hexadienyl benzoate (2) — were studied under oxygen in the presence of cobalt (II) stearate at varying concentrations (0 wt%, 1 wt%, and 5 wt%) and timescales. Due to the complexity of Amosorb® analysis, smaller analogues were prepared and studied. The oxidation products were characterized using ¹H NMR, COSY, GC, LC, and FTIR after exposure to cobalt (II) stearate for 24, 48, and 72 hours. Key findings indicated that both model compounds oxidized in the presence of cobalt (II) stearate. NMR analysis, with cobalt (II) stearate removed, revealed the formation of epoxides — particularly in model compound 2 — and the formation of aldehydes. These results provide insights into the oxidation products formed from the usage of diene esters for the application of food packaging.

Keywords: diene ester, Amosorb®, cobalt (II) stearate, oxygen scavenger, packaging, plastic

1 Introduction

1.1 A brief overview on plastics

Over the past century, plastics have become ubiquitous due to their impressive and versatile properties. Along with their resistance to corrosion, low mass, high durability, strength, ability for transparency, and low toxicity, plastics have low production costs, making them the most widely used materials of modern times. Plastic production consumes the largest amount of crude oil after fuel. In 2022, global plastic production reached a staggering 400.3 million metric tonnes, reflecting a growth of approximately 1.6% compared to the previous year.

Plastics safeguard food from spoilage by acting as a physical barrier against microbes, moisture, and UV light.⁴ Additionally, the packaging prevents physical damage which is crucial for transporting delicate items such as soft fruit. Plastic packaging can also be recycled with a lower energy cost compared to metal or glass packaging materials, and where recycling is not feasible, it is compatible with waste-to-energy disposal.⁴ Most recent research puts the global recycling rate at 9%. In contrast, a huge 57% of plastic waste is directed to landfill, whilst 29% is incinerated and the remaining 6% is mismanaged.⁵

About 40% of plastic produced is single-use plastic - intended for disposal after a short period of time, like sanitary pads, packets, and wrappers to name just a few.⁶ Plastic is also used in transportation like cars to decrease greenhouse gas emissions due to reduction in weight and production impacts compared to other materials.⁷ Furthermore, glass is three times as heavy as plastic, which leads to increased emissions when transporting glass packaged goods due to increased fuel consumption required to transport the heavier glass packaging. Therefore, the

carbon footprint and the consequently negative environmental impact is much higher than plastic packaging. Single-use plastic packaging, therefore, is in many ways the most sustainable packaging option under many circumstances, though it does have significant drawbacks mainly related to the petrochemical origin of most plastics (incompatible with a true circular economy) and the low rate of recycling despite this being technically very feasible in most cases.

1.2 Plastic waste

Plastic waste has and continues to create serious problems including water pollution, environmental damage, and human health problems.⁸ On a global scale, approximately 348 million metric tonnes of plastic waste was generated in the year 2017 and it is predicted that this number will increase four-fold by 2050.⁸ Plastic waste has been littered into water courses and directly into oceans, negatively affecting the biome by impacting sea life and freshwater supplies. Plastic can also act as a conveyor for lipophilic harmful substances like polychlorinated biphenyls (PCBs) and other persistent organic pollutants (POPS), potentially concentrating these pollutants and introducing them into food chains when microplastics are ingested by fish.⁹ Although it must be noted that the sustainability of commercial fishing itself is very questionable, both in terms of ecosystem damage directly by over-harvesting, and because the fishing industry is a major source of oceanic plastic waste, much of which is by design a serious wildlife entanglement hazard.¹⁰

These concerns mean more plastic materials will need to be managed safely going forwards, both in terms of the hazards of additives, but also to ensure recyclability on a systems and supply chain level, and ensure sustainable and circular lifecycles to prevent ocean and land pollution by plastics.

Some of the Sustainable Development Goals (SDGs) in the United Nations 2030 agenda aim to reduce waste generation through prevention, reduction, recycling, and reuse. Along with this, there is a focus on significantly reducing marine pollution, particularly from land-based activities to achieve a circular economy. Plastics, where used responsibly in the context of a circular economy, can in many cases be a sustainable option for many applications, including single-use packaging where they are appropriately designed to be effectively recycled.

Furthermore, plastic innovations like removable labels and easily washable inks further enhance recyclability in comparison to other packaging solutions like metal, paper, and wood. Where metal makes storage efficiency difficult, paper's vulnerability to moisture is exceptionally high and wood is porous and can harbour bacteria.¹²

1.3 PET

An example of a common plastic is polyethylene terephthalate (PET). PET is the fourth most produced plastic after (polypropylene) PP, polyethylene (PE) and polyvinyl chloride (PVC) with annual production capacity of 30.5 million metric tonnes. ^{13, 14} PET is used by manufacturers to produce bottles, food packaging, and textiles. ¹⁵ PET is used widely in food packaging, as it is impermeable to air, allowing the creation of airtight containers that allow food to stay fresher for longer, reducing food waste. As well as this, PET production, recycling, and transport has a significantly lower environmental footprint than glass packaging, and this has resulted in a reduced packaging carbon footprint overall since PET began to replace glass as the most common bottle material. ¹⁶ This has also reduced the carbon footprint over the years, as PET becomes more and more widely used material.

Polyethylene terephthalate (PET) recycling is considered vital to achieving a circular economy of plastic waste.¹⁷ PET bottles do not naturally degrade within a reasonable timescale but persist in the environment for approximately 450 years.¹⁸ If improperly disposed of, they can circulate in soil and oceans, which may cause the release of potentially harmful microplastics, depending on the scenario.^{19, 20} Therefore, ensuring the recyclability of PET packaging is an important part of avoiding ocean microplastics, as part of wider improvements to waste management systems.

Life cycle analysis (LCA) is a comprehensive method used to evaluate the environmental impacts of a product throughout its entire life cycle, from raw material extraction to disposal.

For PET, LCA helps in understanding and mitigating its environmental footprint. LCA for PET involves comparing PET with alternative materials or assessing the impact of different disposal methods like incineration or landfilling. The scope involves defining system boundaries, functional unit (e.g. one PET bottle) along with environmental impact categories assessment that include global warming potential and resource depletion. LCA also helps in comparing PET with other materials like glass and aluminium to determine the most sustainable option. During PET manufacturing, process optimization is performed to identify areas where environmental impact can be minimised, such as reducing energy consumption or improving recyclability. The last stage of LCA encompasses disposal or recycling of the product which is referred to as End-of-Life (EoL).

The primary consideration when applying LCA to assess the end-of-life of PET packaging or its substitution with renewable materials includes the impact analysis methods relevant to the geographic boundaries and the scope of applications for recycled PET. This is due to the regional differences in energy sources, waste

management practices, and regulatory frameworks.²²

An LCA study performed for Coca-Cola Company investigated the use of PET for packaging of soft drinks. The study revealed that plastic bottles have less environmental impact compared to their glass counterparts.²³ This has lead to several technical improvements in PET bottles, including barrier properties, wall thickness and design.²⁴

It was also concluded by the authors that multi-recycling trips, relating to the number of times the same packaging will return for recycling, drastically reduce all the environmental impacts. However it was found that introducing recycled PET into bottles is the best option to reduce all impacts.²⁵

Recycled PET (rPET) flakes and virgin PET flakes are two forms of PET flakes from which products can be made. Virgin PET is produced from raw materials, specifically from purified terephthalic acid (PTA) (or the more soluble methyl ester) and monoethylene glycol (MEG), during the polymerisation process. Virgin PET is commonly used in applications where high-quality material is essential, whereas rPET flakes are made from post-consumer PET products, such as used plastic bottles. The quality of rPET can be more variable than virgin PET, as it depends on the cleanliness and quality of the collected materials, but it supports the circular economy by keeping materials in use longer.

1.3.1 Mechanical recycling

Mechanical recycling of PET involves several key steps to transform used PET products into reusable materials. The steps are: collection, sorting, washing, shredding, drying, extrusion, quality control, and reuse (Figure 1).¹⁵

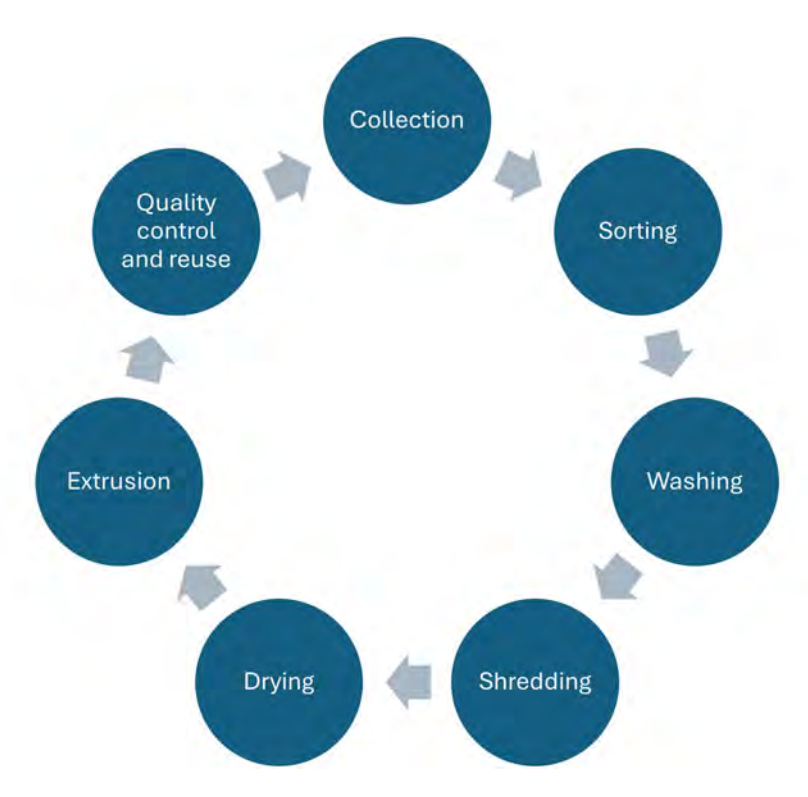


Figure 1: Processes involved in mechanical recycling.

During the collection step, PET bottles and containers are collected through various methods such as kerbside collection, deposit return scheme, and recycling programs. The collected PET waste is then transported to recycling facilities, after which it is sorted to separate PET from other materials. This is achieved using both mechanical sorting methods (like screens and air classifiers) and optical sorting methods (using infrared sensors to identify PET).^{26, 27} The sorted PET is then thoroughly washed to remove contaminants such as labels, adhesives, and residues. This step often involves multiple washing stages to ensure the PET is clean.

The next step is shredding, where the clean PET is shredded into flakes. This increases the surface area and prepares the material for further processing. The following step ensures the flakes are dried to remove any remaining moisture. This is crucial to prevent degradation by hydrolysis during the subsequent melting

process, as this will drastically reduce the molecular weight, leading to degrading rheological and mechanical properties. During extrusion, the dried flakes are melted and extruded into pellets or granules. This involves heating the flakes to high temperatures of 240°C - 280°C which ensures proper melting of PET without causing thermal degradation, then extrusion and chopping to form pellets. In the next step, the recycled PET pellets undergo quality control tests to ensure they meet the required standards for reuse i.e. testing for impurities. This completes the recycling loop, as these new products can eventually be recycled again. PET is also often made from the methyl ester rather than the acid — the ester is more soluble and there are fewer residual acid groups in the final polymer, giving a better product.

Historically, mechanical PET recycling was focused on non-food-grade applications, mainly polyester fibres.³⁰ These fibres are widely used for textiles, carpets, and polyester cord or rope. However, more recently bottle-to-bottle recycling has become much more common. 31 A small 7% is recycled bottle-to-bottle. 32 This is the result of existing technology, mechanical recycling which cannot eliminate colours from PET waste and degrades the material's quality with each cycle, reducing the usability of recycled plastics. Where PET resins are melted, purified and reformed to make more bottles that are of high quality to be reused. For food-grade applications, it has been made a requirement that bottle feedstocks should not contain more than 5% non-food packaging, some producers even use 100% rPET for their bottle production.^{33, 34} This type of recycling is also known as a closed loop system, where it can help to reduce the use of fossil fuels and carbon dioxide emissions.³⁵ However, recycling of food-grade PET is therefore partially possible through mechanical recycling. However, contamination with non-food-grade material and polymer degradation means this is not a truly closed-loop, and most food-contact PET will eventually be "downcycled"

to non-food applications, from which it can no longer return to food-grade use via mechanical recycling methods.

1.3.2 Chemical recycling

Chemical recycling involves breaking down polymeric chains into smaller molecules, such as monomers, to generate fuels and chemicals.³⁶ Pyrolysis and gasification are key methods for recycling plastic into fuel, addressing plastic waste management challenges and positively impacting global energy demand by reducing the energy required for new polymer production.³⁷ Pyrolysis breaks apart polymers at high temperatures (250-700°C) under an inert atmosphere, producing mixed oil.³⁸ It is suitable for waste streams or multilayer films and does not release significant toxic gases in contrast to bio-oil. However, it may lead to poor selectivity, requiring further purification and high energy use.³⁹

Gasification involves partial oxidation to convert plastic waste into H_2/CO syngas. It includes drying, pyrolysis, combustion, cracking, and reduction steps. This process is useful for all polymer types, but involves the release of toxic gases such as nitrogen oxides (NO_x) , sulfur oxides (SO_x) and volatile organic compounds (VOCs). These byproducts contaminate the syngas making it less suitable for monomer production.^{39, 40}

Both pyrolysis and gasification processes are useful for heavily contaminated or mixed polymer waste streams, as any hydrocarbon type materials can be converted to syngas so the presence of other plastics and most residues are well tolerated, but can more properly be thought of as a form of "downcycling" as the products are lower value than the original polymer and not intended for reuse in a similar application. In terms of waste management hierarchy (WMH), this places pyrolysis and gasification lower in the hierarchy compared to mechanical

recycling, which aims to retain the material's value, chemical complexity, and usability. 41

Depolymerisation is the process of converting a polymer back to its component monomers, which may then be purified and re-polymerised to generate new material in theory chemically identical to virgin polymer. However, to be as effective as possible, the material used in this process must all be from the same polymer, or any contaminant must tolerate and be tolerated by the depolymerisation conditions. However, contaminated waste streams can result in mixtures of monomers or complicate purification, making effective recovery and monomer re-use difficult in practice. To attain sufficiently high molecular weight polymers, monomers must be very pure as any trace impurity has the potential to end-cap growing polymer chains, or terminate radicals, depending on the polymerisation type, drastically reducing molecular weight.

This is where post-industrial recycling (PIR) and post-consumer recycling (PCR) differ: with PIR it is much easier to gather together items of the same polymer as industrial waste streams are better defined and less likely to be contaminated with unknown materials. With consumer recycling systems, it is common to have a wide mix of plastics in one batch of materials to be recycled, and for the contamination profile to be variable and undefined. This makes PCR content problematic for food packaging applications, requiring further processing in order to be food safe.⁴⁴ An example might be the case where non-food materials, including some genuinely hazardous chemicals such as pesticides, might be stored in repurposed drinks bottles which then enter the recycling system at the kerbside. This clearly poses risks to bottle-to-bottle mechanical recycling.

1.4 Food waste and food packaging

In 2019, approximately 932 million metric tonnes of food waste were generated globally by consumers, especially by high-income countries.⁴⁵ On top of this, each year more than 1.3 billion metric tonnes of food are discarded through the food supply chain worldwide; this is more than a quarter of the total global agricultural production.⁴⁶ It can be predicted that the rate at which food degrades is an influencing factor for wasted food. Research conducted by the United Nations reports that more than 920 million metric tonnes of food sold in 2019 was discarded into waste bins.⁴⁷ Therefore, the importance of packaging chemistry is vital in extending the shelf life of food. According to the United Nations Food and Agriculture Organisation (UNFAO), 13.2% of food is lost globally after harvest on farm and in storage, as well in transport. In addition to this, 19% is wasted at retail and household levels.⁴⁸ Much of this is lost as a result of food being spoiled or expired.⁴⁹

There are a number of methods used in the preservation of food and ensuring high quality standards of the packaged content. For example, oxygen permeability determines how easily oxygen passes through a packaging material, allowing for the measurement of oxygen transmission rate (OTR), expressed in cm³ · m⁻² · s⁻¹.⁵⁰ Therefore, the lower the oxygen permeability and OTR, the better the packaging materials in protecting food from oxygen damage.⁵¹ Water vapour permeability (WVP) is also very important in food applications as the lower the water vapour, the better the packaging barrier in protecting the food against moisture. The water vapour permeability coefficient (WVPC) allows for the quantification of the water vapour barrier, which indicates the amount of water vapour that permeates per unit of area and time in a packaging material, expressed in the units kg mm⁻² s⁻¹ Pa⁻¹.⁵² This is important both to prevent the unintentional drying

out of fresh food items, and the ingress of water creating conditions for spoilage or microbial growth in dry food items.

Modified atmospheric packaging (MAP) is another method to extend shelf life by using controlled mixtures of gases. Some of these gases include nitrogen (N_2) and carbon dioxide (CO_2) and sometimes oxygen (O_2) , With equilibrium, the normal atmosphere outside the packaging does not influence the addition of these mixtures of gases.⁵³ This equilibrium is maintained through various parameters such as gas transmission rates like OTR and WVTR.

1.4.1 Active packaging

Active packaging is the incorporation of certain additives into the packaging system to maintain the product's quality or prolong its shelf life; the additives are placed either loose within the packaging, attached to inner layers of the material or incorporated within the packaging material itself.^{54, 55} Active packaging can be classified into two categories: the first is non-migratory active packaging, which refers to scavengers designed to remove unwanted components from the inside environment of a packaging without intentional migration. The second is active release packaging, which primarily refers to emitters that allow controlled migration of desired components into the packaging environment. Most of the non-migratory active packaging in food can act as an oxygen scavenger, moisture scavenger, and ethylene absorber. Ethylene absorbers, are used to manage levels of ethylene gas, a plant hormone that is responsible for delaying fruit ripening.⁵⁶ Therefore, the controlled use of ethylene can help extend the shelf life of fruits. Furthermore, active-release packaging includes carbon dioxide emitters, antimicrobial packaging, and antioxidant packaging.⁵⁵ The developments of these technologies are constantly advancing, leading to higher food safety and quality standards as well as waste minimization and sustainability.

In recent years, the packaging industry has integrated eco-friendly materials, innovative designs, and lightweight containers. These changes have improved supply chain performance and goods delivery, benefiting both end users and the environment.⁵⁷ However, the increased complexity of packaging can come at the expense of efficient recycling or of recyclability at all.

1.5 Oxygen scavengers

Oxygen contributes to the spoilage of preserved food and beverages through both direct oxidation and by encouraging the growth of aerobic organisms.⁵⁸ There are many ways oxygen may enter packaging: through poorly sealed packaging material, air contained in the containers, diffusion of oxygen through packaging materials themselves, and deficient gas flushing.⁵⁹

Oxygen scavengers are a type of active packaging technology, the most common of which is ferrous oxide. They can be present as sachets or incorporated into the packaging material.⁶⁰ Scavengers work by reducing oxygen concentration in the local environment by sequestering it, thereby inhibiting oxidative reactions which could lead to deterioration of the quality of food and reduced shelf life. For example, it was found that the use of highest capacity oxygen scavenger extended the shelf life of bread products from 3-4 days to 12 days, improving supply chain management for retailers and reducing food waste.⁶¹

Foods like whole grains, nuts and seeds, and plant-based milks to name a few are susceptible to oxygen, meaning that after a prolonged period the food may deteriorate or spoil and become prone to the growth of microorganisms. This puts further emphasis on the importance of controlling oxygen levels in food packaging so that it can positively influence the reduction of food waste.

Oxygen absorbers are typically activated by moisture, which initiates the oxygen absorption reaction.⁵⁸ This moisture can originate either from the food product itself, particularly in the case of moist or semi-moist foods, or from the surrounding atmosphere once the packaging is opened.⁶² Furthermore, when an oxygen absorber is removed from its protective packaging, the moisture in the surrounding atmosphere begins to permeate the particles inside the absorber.

There are two types of oxygen absorbers: ferrous and non-ferrous absorbers. Ferrous absorbers contain iron powder (ferrous iron) and a salt, such as sodium chloride, which is a catalyst in the reaction and has the purpose of accelerating the reaction, even in low-humidity environments. Once iron oxidises, iron oxide is formed (rust). This chemical reaction effectively removes oxygen from the surrounding environments reducing oxygen levels.⁵⁸ By removing oxygen, they help to prevent oxidation of oils and fats as well as preserve colour, flavour, and quality of food.

Non-ferrous absorbers are more commonly used to remove oxygen from sealed environments, and utilise metal-based compounds. Copper and cobalt are examples of metal-based compounds used for this application. Similar to iron-based absorbers, nonferrous absorbers work by reacting with oxygen to form stable compounds, effectively reducing oxygen content from inside of the packaging, and therefore increasing the shelf life of food.⁶³

1.5.1 Oxygen scavengers within films

PET has excellent barrier properties and high transparency, ideal for packaging that intends to show the food from the outside. Oxygen scavengers embedded into films are preferred for liquid substances as opposed to oxygen-absorber sachets which are not appropriate due to spillage of sachet content or soaking of the sachet in the liquid, either of which can easily contaminate the food.

The packing structure portraying how well the film works to protect the food from oxygen is shown in Figure 2. This material is embedded into a layer that is permeable to oxygen, and it can therefore absorb oxygen present. The rate and amount of oxygen ingression can then be measured. Some other methods of making a PET film capable of decreasing oxygen content and increasing food quality include applying an active layer to the package surface, incorporating active compounds into the polymeric matrix of the packaging, and the use of immobilized active films.⁶⁴ Multi-layer active packaging films are designed to absorb oxygen coming from inside and outside of the packaging. For example, polyamide-based oxygen absorbing films are used as active additives to oxygen scavenging films, to absorb oxygen inside of packaging, and oxygen coming from the outside environment is controlled by polylactic acid (PLA).⁶⁴

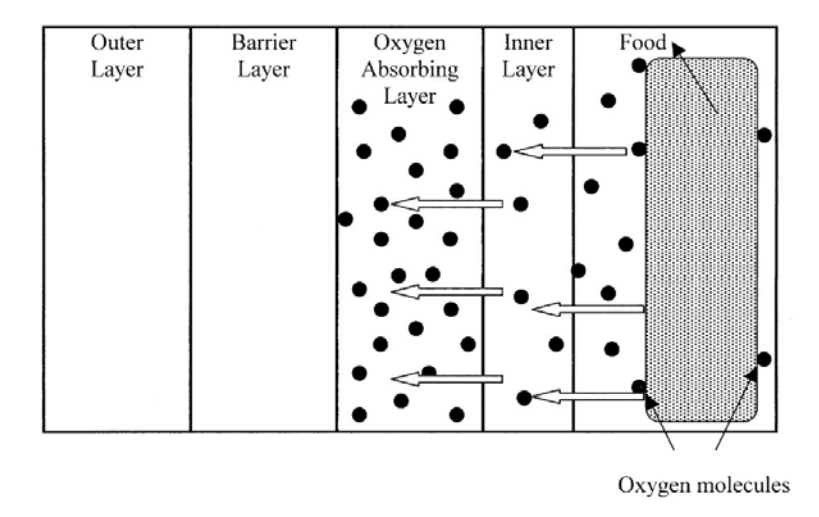


Figure 2: Typical structure of oxygen-absorbing multi-layer active packaging films. ⁶⁵ Reproduced from *Active Food Packaging Technologies* by Murat Ozdemir and John D. Floros in *Critical Reviews in Food Science & Nutrition*. © Copyright 2004. Reprinted by permission of Informa UK Limited, trading as Taylor & Francis Group. ⁶⁶

Modification of the polymer chain provides many opportunities to introduce oxygen scavengers, including the addition of oligomers (the chain of which can break when reacted with oxygen, or a side chain can do the same), or the introduction of unsaturated sites within a polymer chain which can then react with oxygen. Another interesting development is the use of nanocrystalline titania into polymer matrixes, where oxygen is absorbed when the material is exposed to UV light. However, in a food packaging application, the product is likely to be indoors or covered the majority of the time, and therefore wouldn't be exposed to UV light for long durations, if at all.⁶⁴

There are other types of films known as polyamide-based oxygen-absorbing films. These incorporate cobalt catalysts and MXD-6 nylon polymers (Figure 3) which have been commercialised as reactive oxygen-scavenging barriers when incorporated into multilayer polymeric packaging structures.⁶⁴

Figure 3: Structure of nylon MXD6.⁶⁷

1.6 Amosorb®

Amosorb® is a copolymer (Figure 4) formed by transesterification.⁶⁸ This copolymer has a high oxygen transmission rate (OTR), meaning that oxygen permeates through the barriers of PET. This is due to the effectiveness of oxygen scavengers, which are the copolycondensates derived after the condensation of the copolymer.⁶⁸ The compositions that make up the copolymer have a strong tendency to absorb oxygen. This enables the purpose of the packaging – extending the shelf life of food.

Figure 4: Structure of the oxygen-scavenging condensation copolymer showing polyethylene terephthalate (PET) monomer, pyromellitic dianhydride (PMDA) linker, and polybutadiene (PBD) polymer group (highlighted in blue).

This copolymer combines PET (or PET oligomer) segments with polybutadiene (PBD) and is incorporated into PET packaging alongside a cobalt (II) stearate catalyst.⁶⁸ This material is prepared by a reactive extrusion process where chain scission of PET (likely promoted partially by the cobalt) and subsequent copolymerisation of the PBD segments via the linkers occurs in situ during co-extrusion.⁶⁸ This material is then added to PET products.⁶⁸ The mechanism of action is believed to involve the oxidation of the PBD alkenes in the presence of cobalt. However, the detailed mechanism and nature of oxidation products is difficult to elucidate due to the complex (and to some extent, random) structure of the Amosorb® copolymer, which defies straightforward analysis. Nevertheless, Amosorb® is an effective oxygen scavenging additive, and has been used commercially for many years.⁶⁸

1.6.1 Problems with Amosorb®

Amosorb® has several problems, however, which limit its abilities in acting as an oxygen scavenger for food packaging. Firstly, the copolymer is prone to going yellow upon storage as well as when the material is heated for recycling, both of which limit the recyclability of Amosorb®-containing packaging. In addition to this, the nature of the oxidation is not understood in terms of how the polyenes

scavenge oxygen, therefore, research into understanding how oxidation impacts a model version of the Amosorb® would extend knowledge in the field and likely permit a more optimal implementation of the technology. Finally, reliability issues with the incorporation of Amosorb® within film packaging were identified.

1.7 Project aims

The key aims of this project are to:

- Prepare a small molecule analogue model compound 1 (Figure 5), which
 is based on the key structural features of Amosorb® and expose it to oxygen in order to better understand the oxygen-scavenging chemistry involved
 and the conditions under which this works.
- Replicate and understand the chemistry responsible for the yellowing of Amosorb®-containing materials on prolonged storage or when heated following storage.

Figure 5: Trans-2,4-hexadienyl acetate (model compound 1).

2 Experimental

2.1 Reagents and Chemicals

Trans-2,4-hexadiene-1-ol, 99%, stabilised with 0.1% -tocopherol, (Thermo Scientific); Cobalt (II) stearate, >97.7%, (Tokyo Chemical Industry UK Ltd.); Dichloromethane (DCM), anhydrous 99.7+%, stab. with amylene (Thermo Scientific); potassium hydroxide (KOH) (Thermo Scientific). All other chemicals were purchased from Thermo Fisher scientific and were Analytical Reagent grade unless otherwise specified.

2.2 Instrumental analysis

NMR spectroscopy: The NMR spectra including ¹H NMR, ¹³C NMR, ¹H/¹H-correlation spectroscopy (¹H/¹H-COSY), ¹H/¹³C-hetero nuclear single-bond correlation spectroscopy, were recorded using a 500 MHz JEOL spectrometer (JEOL, Spain) at 125 MHz. The chemical shifts for ¹H and ¹³C NMR spectra were referenced to the residual solvent peak of deuterated methylene chloride at 5.32 ppm for the ¹H NMR spectra and 54.24 ppm for ¹³C NMR spectrum. NMR spectra were processed using MNOVA software from MestreLab research, Spain.

IR spectroscopy: Infra-red analysis was performed using a Thermo-Scientific Nicolet iSIOATR – FTIR instrument (Thermoscientific, Rochester, USA) using a resolution of 4 cm⁻¹.

Thin layer chromatography (TLC): TLC was performed on Silica gel 60

F254, supplied by Sigma-Aldrich. TLC plates were visualised under UV light

and by staining with potassium permanganate (solution in aqueous sodium car-

bonate).

High performance liquid chromatography (HPLC): LC data was collected

using Agilent 1260 Infinity HPLC with an ESI ionisation in positive mode. The

data was processed using OpenLab CDS software.

Gas chromatography mass spectroscopy (GCMS): GC data was collected

using the Agilent 5977C GC system with the Agilent 19091S-433UI column (di-

mensions 30 m x 250 μ x 0.25 μm). The detector was a single quadrupole mass

selective detector (MSD). Helium was used as the carrier gas. The data was

analysed using the Agilent MassHunter® software.

Model compound 1 (Figure 6) was then synthesised. In this reaction, acetyl

chloride (5.45 g, 69.44 mmol) was added dropwise to a solution of trans 2,4-

hexadiene-1-ol (5 g, 50.94 mmol) and triethylamine (5.34 g, 52.77 mmol, 1.5 eq)

in anhydrous DCM (100 mL) at 0°C, then allowed to warm to room temperature.

The mixture was stirred at room temperature for 2 hours and was monitored

via TLC (eluting in petroleum ether and ethyl acetate in a 5:1 ratio) until the

starting material had been fully consumed. The organic layer was washed with

diluted 2 M NaHCO₃ (3x 10 mL), water (3 x 10 mL), and brine (3 x 10 mL)

and then dried over anhydrous MgSO₄. The solvent was removed under reduced

pressure, and the crude product was purified using column chromatography (silica

gel, petroleum ether/ethyl acetate (15:1)) to afford the product as a yellow oil (5

g, 35.31 mmol, 70%).

Rf (PEt:EtOAc 10:1) – 0.34

Page 21 of 71

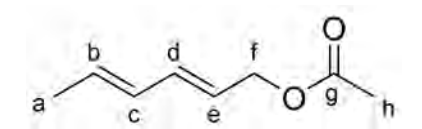


Figure 6: Labelled structure of model compound 1.69

IR cm⁻¹ $\sim 3100 \text{ (Sp}^2 \text{ C-H stretch)}, 2967 \text{ (Sp}^3 \text{ C-H stretch)} - 1734 \text{ (C=O stretch)}, 1661 \text{ (C=C stretch)}, 1220 \text{ (C-O stretch)}, 3673 \text{ (O-H stretch)}.$

¹H NMR (500 MHz, DEUTERATED METHYLENE CHLORIDE)

6.3 - 6.2 (dd, J = 10.4, 15.3 Hz, 1 H, \mathbf{d}), 6.1 - 6.0 (ddd, J = 10.6, 13.3 Hz, 1 H, \mathbf{c}), 5.8 - 5.7 (dq, J = 6.7, 13.8 Hz, 1 H, \mathbf{b}), 5.6 - 5.5 (dt, 1 H, \mathbf{e}), 4.5 (d, J = 6.6 Hz, 2 H, \mathbf{f}), 2.0 (s, 3 H, \mathbf{g}), 1.8 (d, J = 6.6 Hz, 3 H, \mathbf{a}). See Figure A1.

¹³C NMR (126 MHz, DEUTERATED METHYLENE CHLORIDE)
170.6 (g), 134.5 (d), 131.2 (b), 130.4 (c), 124.0 (e), 64.8 (f), 20.8 (h), 17.9 (a).
Assigned using HSQC (Figure A2).

Model compound 2 (Figure 7) was then synthesised. In this reaction, benzoyl chloride (1.763 g, 1.25 mmol) was added dropwise to a solution of trans 2,4-hexadiene-1-ol (1 g, 10.23 mmol) and triethylamine (1.075 mL, 8.10 mmol, 1.5 eq) in anhydrous DCM (100 mL) at 0°C, then allowed to warm to room temperature. The mixture was stirred at room temperature for 3 hours and was monitored via TLC until the starting material had been fully consumed. The organic layer was washed with diluted 2 M NaHCO₃ (3 x 10 mL), water (3 x 10 mL) and brine (3 x 10 mL), dried over anhydrous MgSO₄. The solvent was removed under reduced pressure, and the crude product was purified using column chromatography (silica gel, petroleum ether/ethyl acetate (4:1)) to afford the product as a yellow oil (0.4473 g, 2.2116 mmol, 98% yield obtained prior to column).

Rf (PET:EtOAc 4:1)

$$\begin{array}{c|c} a & O & h & J \\ \hline & & & \\ b & & d & \\ \end{array}$$

Figure 7: Trans-2,4-hexadienyl benzoate (model compound $\mathbf{2}$)⁷⁰

IR cm⁻¹: 3100 (Sp² C-H stretch), 2934 (Sp³ C-H stretch), 1714 (C=O stretch), 1583 (C=C stretch), 1490 (C=C stretch), 1264 (C-O stretch in ester)

¹H NMR (500 MHz, DEUTERATED CHLOROFORM) 8.1 (dd, J = 8.1, 1.5 Hz, 2 H, \mathbf{f}), 7.6 – 7.5 (t, J = 7.4, 7.4 Hz, 1 H, \mathbf{b}), 7.4 (t, J = 7.7 Hz, 2 H, \mathbf{a}), 6.3 (dd, J = 15.3, 10.4 Hz, 1 H, \mathbf{j}), 6.1 (dd, J = 12.3, 15.0 Hz, 1 H, \mathbf{k}), 5.8 – 5.7 (m, 2 H, \mathbf{i} and \mathbf{l}), 4.8 (d, J = 6.6 Hz, 2 H, \mathbf{h}), 1.8 (d, J = 6.6 Hz, 3 H, \mathbf{m}). See Figure A3.

13C NMR (126 MHz, DEUTERATED CHLOROFORM) 166.5 (g),
135.1 (j), 133.0 (b), 131.4 (l), 130.6 (k), 129.7 (f and d), 129.1 (e), 128.4 (a,c),
123.9 (i), 65.5 (h), 18.2 (m). Assigned using HSQC (Figure A4).

Oxidation test method: Solutions of model compound (50 mg/mL) and cobalt (II) stearate (100 mg/mL in anhydrous DCM) were prepared and dosed accurately in the appropriate ratios into a glass vial. Solutions were then dried under a stream of nitrogen before being exposed to dry air in a desiccator over potassium hydroxide for the appropriate duration. Samples were characterised by 1H NMR immediately after the correct time had elapsed. For further analysis not immediately available, samples were flushed thoroughly with dry nitrogen and stored sealed at 4°C until analysis was carried out to avoid additional oxidation. Cobalt (II) stearate is part of the Amosorb® formulation, and is believed to promote oxidation of the alkenes, so it was included in the model system.

3 Results and Discussion

3.1 Model Compound 1

Model compound 1 (Figure 8) was designed as the simplest small molecule analogue which, in combination with cobalt (II) stearate (Figure 9), would contain all of the functionality believed to be present in the active Amosorb® copolymer. It contains an ester group (highlighted in blue and an oxidisable conjugated diene (highlighted in orange) analogous to the polybutadiene segment of Amosorb®. In addition to this, the Amosorb® may contain small amounts of diene units, which are present in model compound 1, making it more easily oxidisable, justifying the choice of a diene ester as a model.

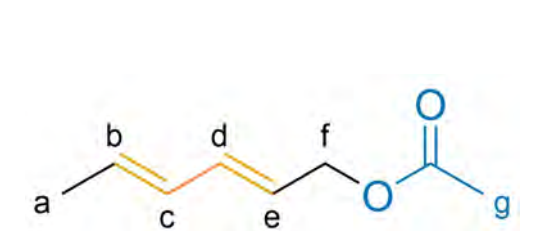


Figure 8: Chemical structure of model compound 1 (trans-2,4-hexadienyl acetate).

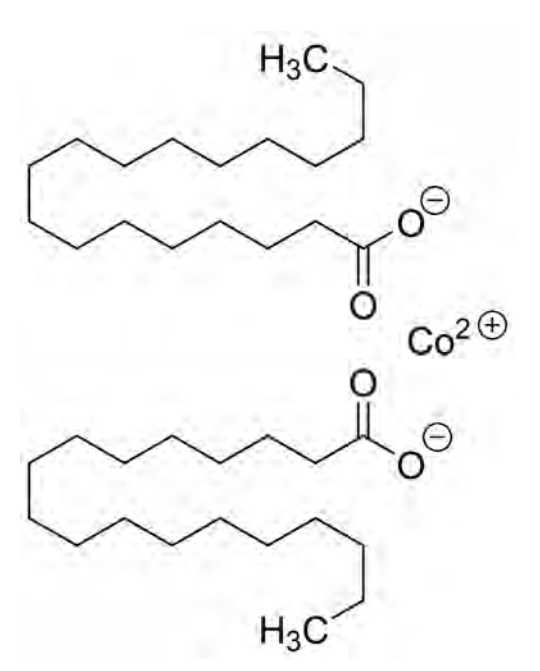


Figure 9: Chemical structure of cobalt stearate.

3.1.1 Synthesis

The synthesis of model compound 1 was achieved by the reaction of trans-2,4-hexadiene-1-ol with acetyl chloride and a base triethylamine, all dissolved in DCM (Scheme 1).

$$H_3C$$
 OH + H_3C CI O NEt₃ O DCM, ~ 2 h

Scheme 1: Reaction scheme for the synthesis of model compound 1.

The synthesis of model compound 1 was successful with a yield of 70%, which was sufficient to validate the use of model compound 1 for the oxidation experiments.

3.1.2 Oxidation of model compound 1

The commercial formulation of Amosorb® contains cobalt stearate, as well as likely playing a role in the co-polymerisation reaction as it is believed to promote oxidation of the alkenes. Cobalt (II) stearate was therefore included at different levels in model oxygen scavenging experiments. Preliminary experiments and the experience of colleagues at Avient™ working with Amosorb®, indicated that cobalt (II) stearate is sensitive to moisture, forming complexes with water which are known to be inactive. In Amosorb® formulations, this is mitigated by the effective encapsulation of the Amosorb® copolymer within PET, acting as a barrier to atmospheric moisture. However, since it was necessary to keep our model system as simple as possible to enable effective analysis, oxidation experiments were carried out in dry air within a desiccator over potassium hydroxide pellets.

The effect of different concentrations of cobalt (II) stearate on the oxidation of model compound 1 is shown in Figures 10 to 12. It is clear from the ¹H NMR data that cobalt (II) stearate can slightly increase oxidation of model compound 1 as

seen from the peaks upfield of the CH₃ signal. This result has also been found in studies with polymer systems.⁷¹ However, after each of the three time intervals of 24, 48, and 72 h, very similar changes were observed across the different concentrations of cobalt (II) stearate. The ¹H NMR spectrum of the model compound 1 was the same as the "oxidised" sample with 0 wt% cobalt (II) stearate. However, the samples with different non-zero concentrations of cobalt (II) stearate showed a broadening of all the model compound 1 peaks, so as expected cobalt (II) stearate is promoting oxidation of model compound 1.

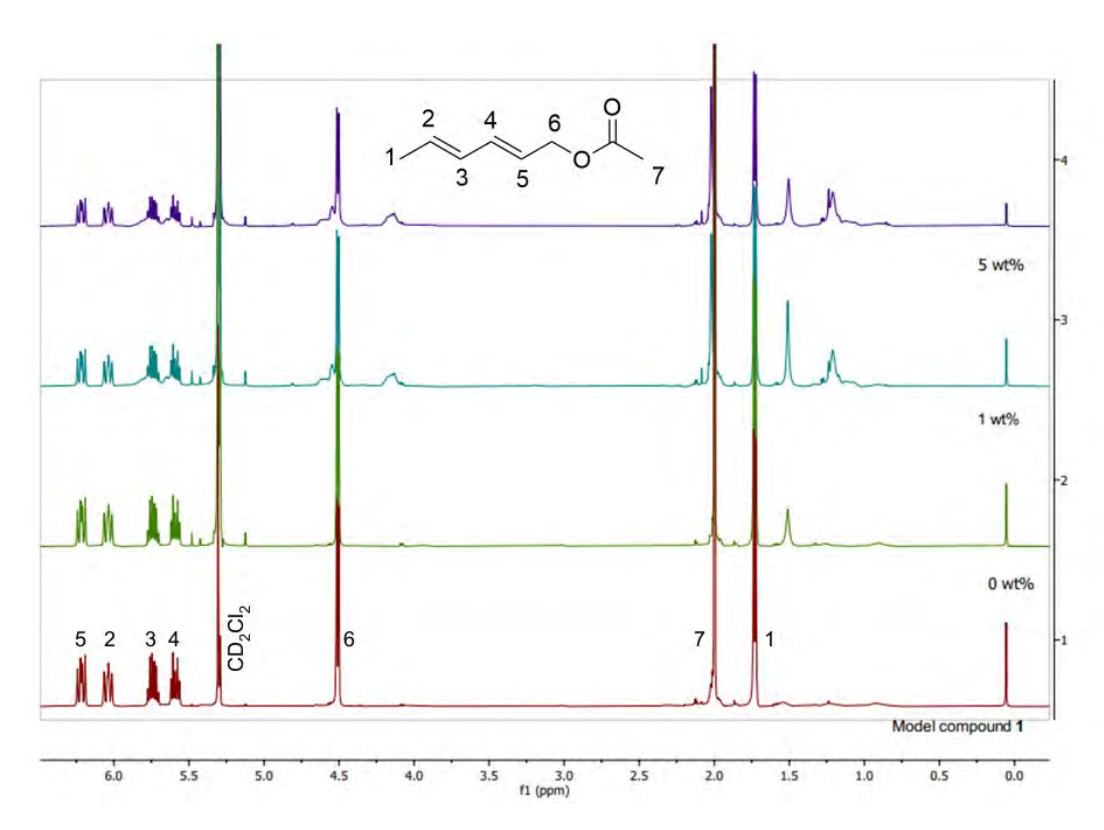


Figure 10: ¹H NMR spectrum of the 24 h exposure samples in the presence of cobalt (II) stearate at different concentrations (wt%).

It was predicted that, upon oxidation, the alkenes would react with oxygen and result in these bonds breaking, leading to changes in the NMR spectra for protons 2, 3, 4, and 5. Groups such as epoxides, alcohols, and aldehydes would appear in the ¹H NMR spectra for oxidised samples. There were no signals detected at the region 10 to 11 ppm, suggesting peroxides and hydroperoxides were not present.

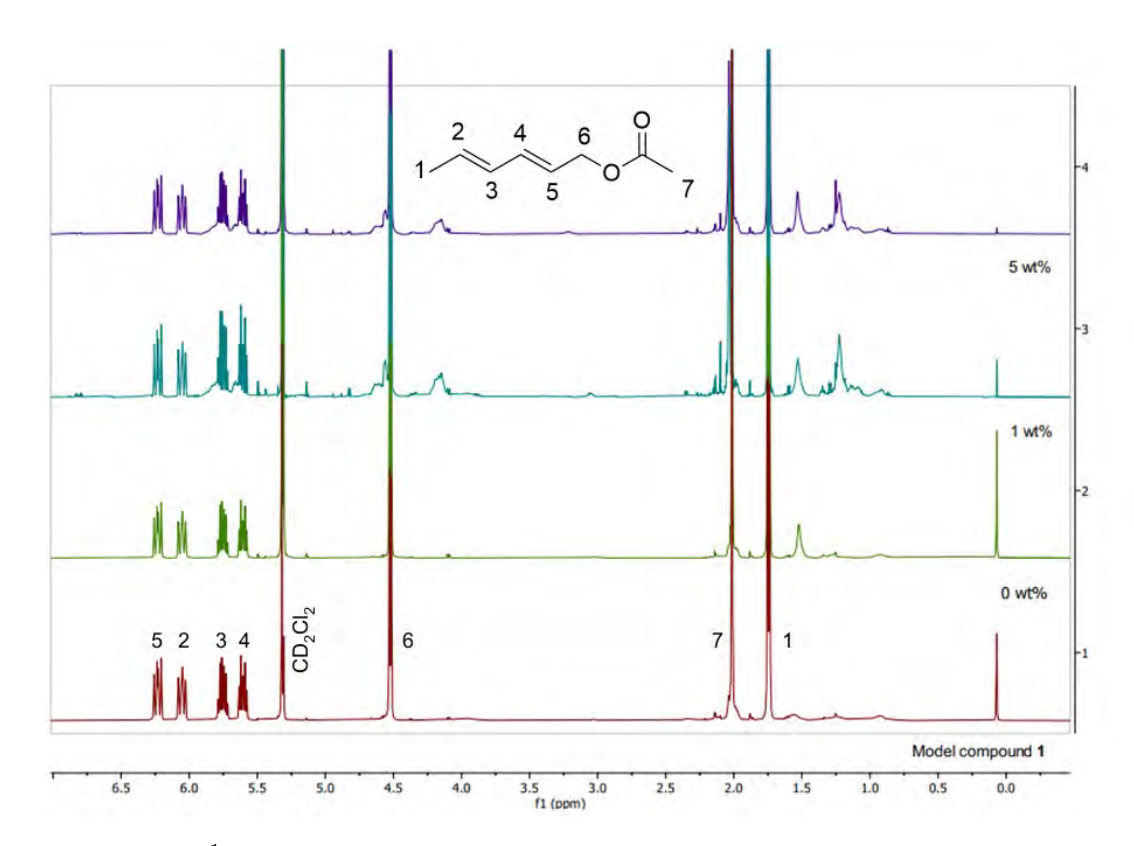


Figure 11: ¹H NMR spectrum of the 48 h exposure samples in the presence of cobalt (II) stearate at different concentrations (wt%).

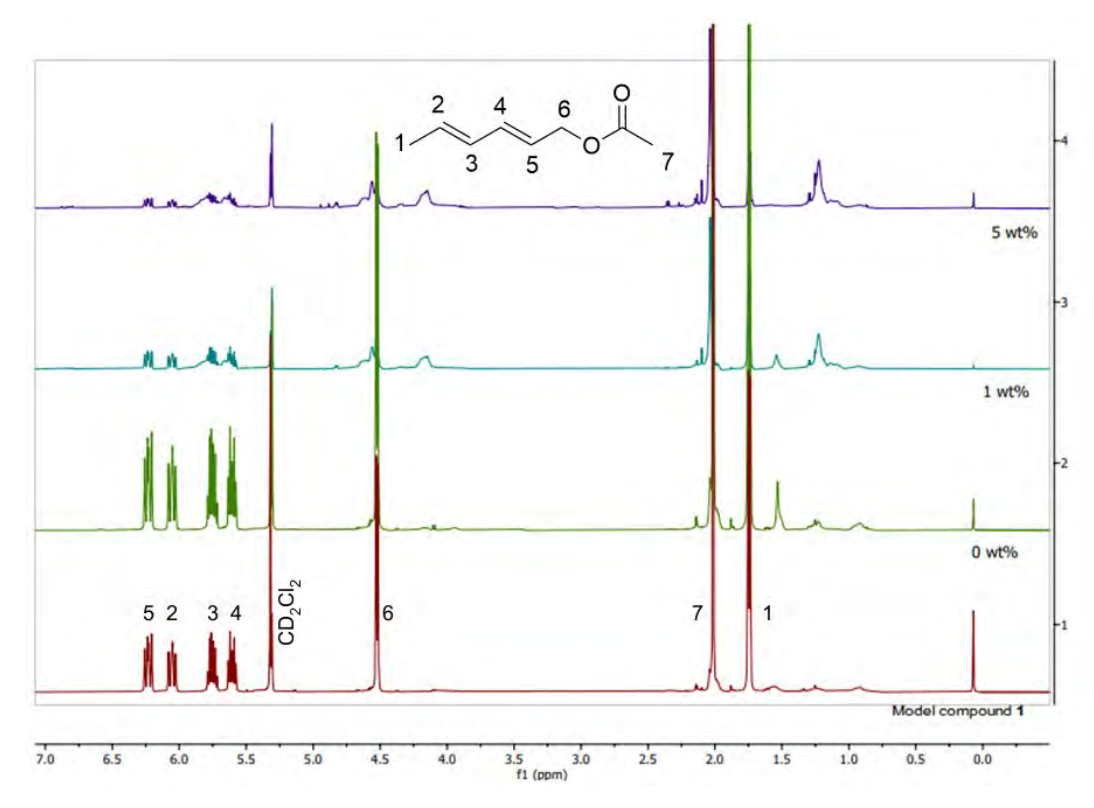


Figure 12: ¹H NMR spectrum of the 72 h exposure samples in the presence of cobalt (II) stearate at different concentrations (wt%). See full spectra in Figures A5 to A7.

However, there are weak signals in the 2.5 to 3.5 ppm region, where normally epoxide peaks would appear. This is consistent with the formation of an epoxide, but not definitive. This was found to be present for 24, 48, and 72 h oxidation experiments. A zoomed-in spectrum of this region is presented in Figure 13.

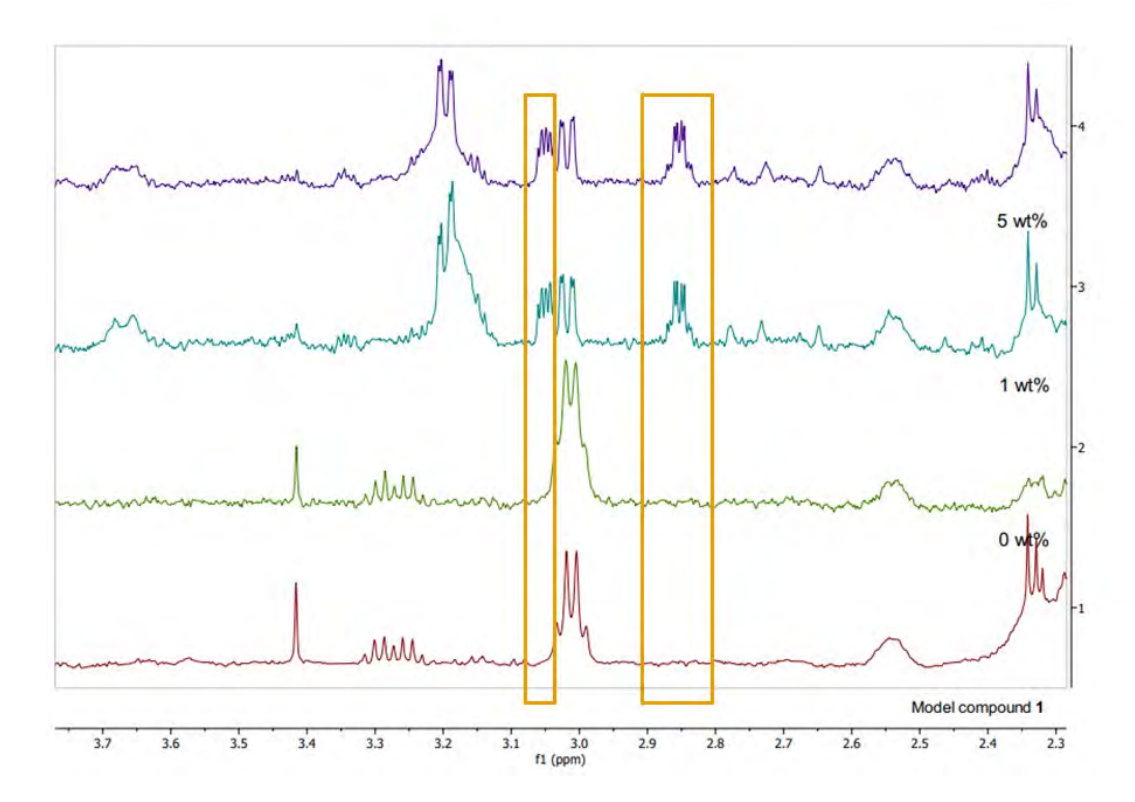


Figure 13: Expansion region showing the development of the epoxide in all the three different concentrations of cobalt (II) stearate at 72 h.

The possible structure of the oxidation product derived from model compound ${\bf 1}$ includes an epoxide ring (Figure 14) at protons H_d and H_e .

The peak H_d at 3.05 ppm integrates to 0.10 protons and the peak H_e at 2.86 ppm integrates to 0.06 protons. There could possibly be two epoxides with a splitting pattern of a quartet and a triplet. The NMR clearly shows a quartet at 2.86 ppm, which aligns with the postulated product. The alkene protons that correspond to the formation of this epoxy ring are the adjacent protons H_a and H_b .

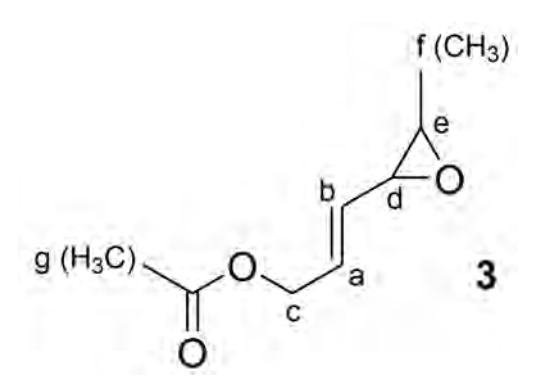


Figure 14: A possible structure of the epoxidated compound (3) derived from model compound 1.

The peak H_a at 6.05 ppm and H_b at 5.60 ppm both have a strong coupling constant of 15.16 Hz and 6.45 Hz, respectively. They both also integrated to 1 proton. There were no signals for (-OH) peaks at the regions 10 to 12 ppm, but this is not surprising as OH peaks are often not seen due to proton/deuterium exchange. This provides support for the presence of the trans-epoxy ring, confirming the successful epoxidation of model compound 1. The ¹H NMR assignment of the trans-epoxy ring was almost identical to that presented in the literature, providing further evidence for the assignment of protons H_d and H_e .⁷²

A significant number of attempts were made to isolate the product of oxidation, to allow analysis of the pure compound (compound 3), including via column chromatography, but were ultimately unsuccessful.

3.1.3 FTIR spectral analysis

An FTIR spectrum of model compound 1 was taken as a baseline comparison to the oxidised samples (Figure 15). It has all the functional groups that are expected to arise from model compound 1. The FTIR spectra of oxidised samples are shown in Figures 16 to 18.

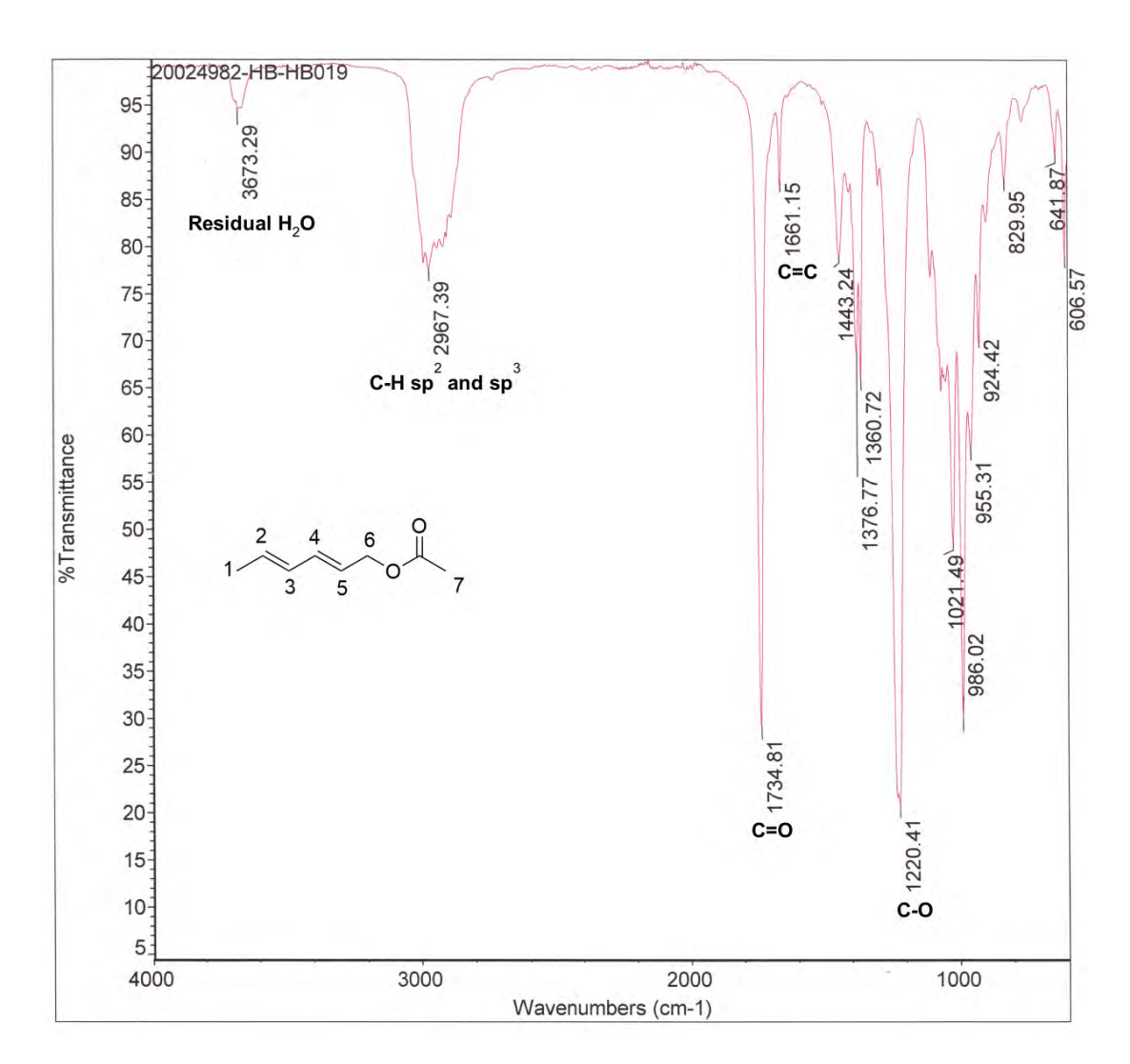


Figure 15: FTIR spectrum of model compound 1.

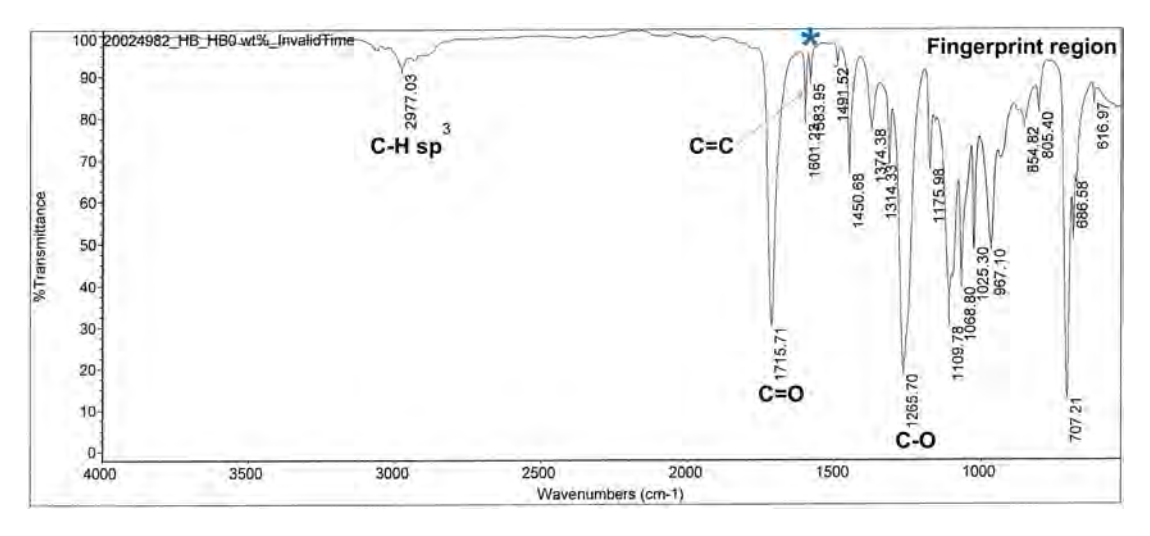


Figure 16: FTIR spectrum of an oxidised sample with 0 wt% cobalt (II) stearate at 96 h exposure.

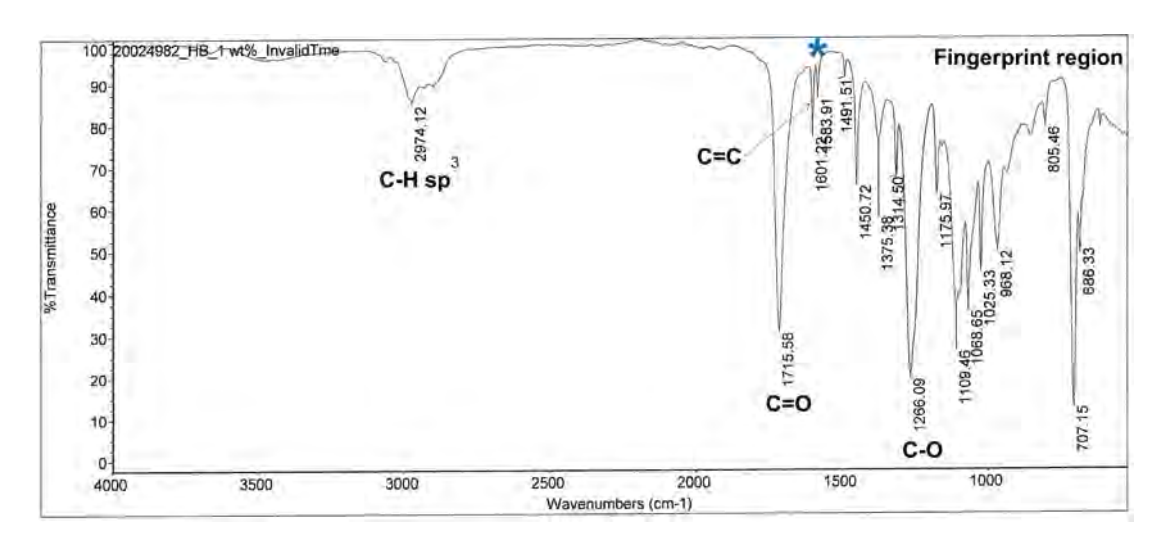


Figure 17: FTIR spectrum of an oxidised sample with 1 wt% cobalt (II) stearate at 96 h exposure.

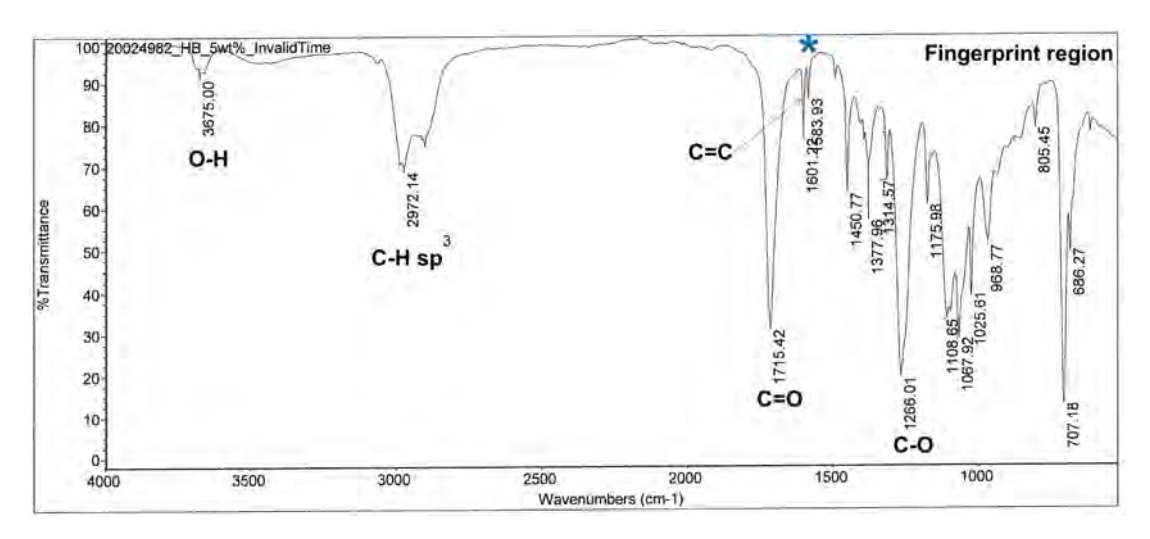


Figure 18: FTIR spectrum of an oxidised sample with 5 wt% cobalt (II) stearate at 96 h exposure.

Unfortunately, no significant changes were observable in the infra-red spectrum of the oxidised material Figures A8 to A9. However, this is not entirely unexpected as epoxides, the most likely candidate oxidation product, appear at around 900 cm⁻¹, where small signals corresponding to partial oxidation are likely buried under signals present in model compound 1. A new small signal is notable at 1583 cm⁻¹ (marked with a star in Figures 16 to 18) but this is difficult to assign with any confidence. The peak at 1109 cm⁻¹ could be attributed to the stearate C–O bond, which is consistent with the IR spectrum from the 5 wt% sample.

After 96 hours, an O-H stretch at 3675 cm⁻¹ is observable for the 5 wt% sample in the IR spectrum (Figure 18). It is unclear whether this is incidental moisture or the epoxide has opened to form a diol. The peak could be residual water, but this is unlikely as the reaction was run dry. The ¹H NMR further backs this statement, as there would be a peak at 1.5 ppm if water was present but there is not, especially for the 5 wt% sample at 72 h (Figure 12). There is evidence however that it may be an epoxide and the ¹H NMR evidence backs this (Figure 13). Therefore, it is more likely that the epoxide opened to form a diol.

3.1.4 LC-MS analysis

To further characterise and understand the molecular mass of the oxidised samples, liquid chromatography mass spectrometry (LC-MS) was used. Figures 19 to 21 show chromatograms achieved for samples with 0 wt%, 1 wt%, 5 wt% cobalt (II) stearate. The chromatograms shown are only for the 24 h samples because ionising the oxidised samples using electrospray ionisation was unsuccessful, so no correct masses were identified from the mass spectrum.

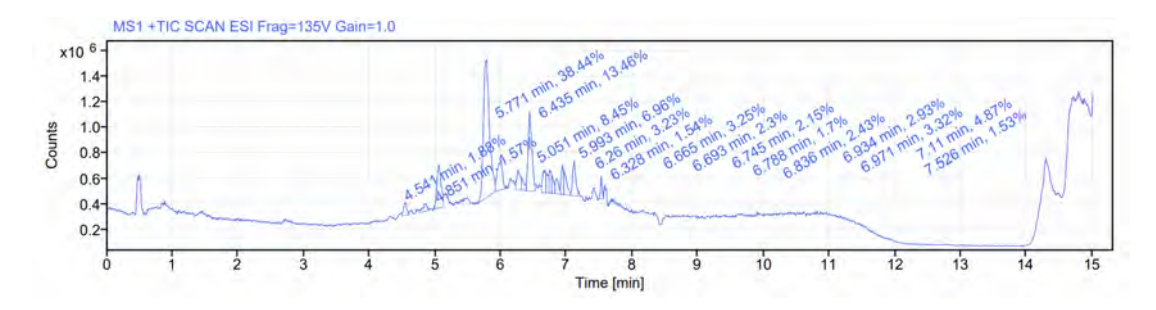


Figure 19: LC chromatogram of the 24 h sample without cobalt (II) stearate.

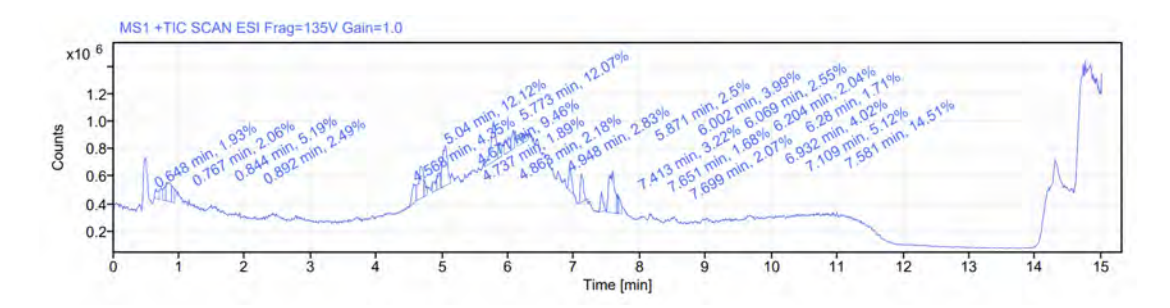


Figure 20: LC chromatogram of the 24 h sample with 1 wt% cobalt (II) stearate.

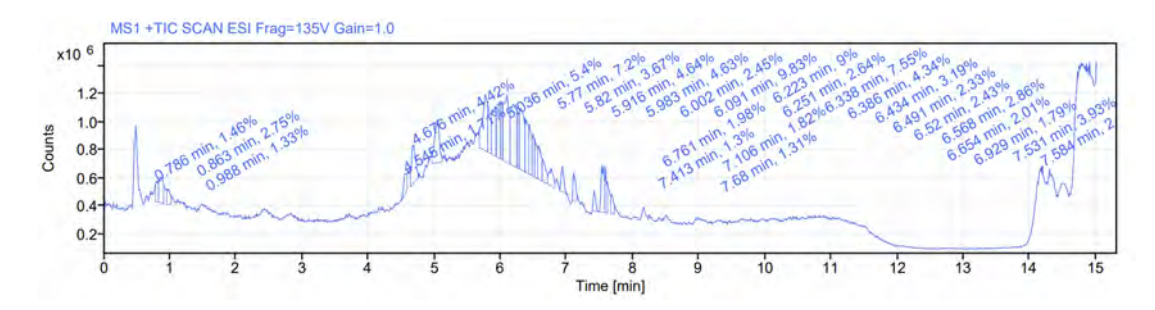


Figure 21: LC chromatogram of the 24 h sample with 5 wt% cobalt (II) stearate.

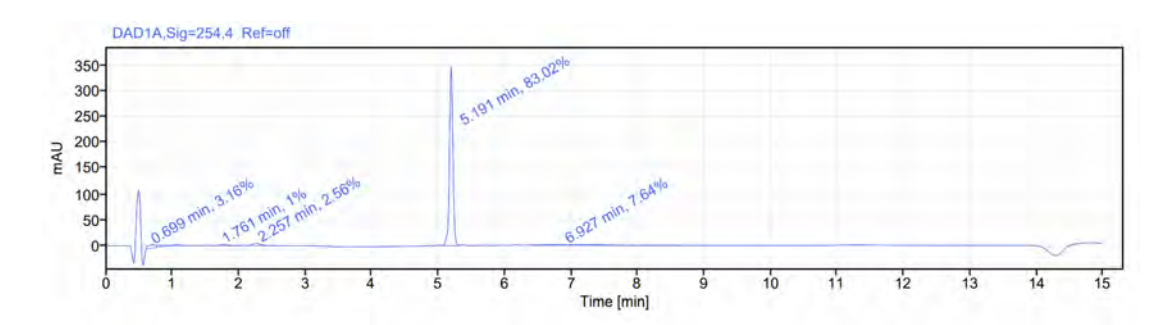


Figure 22: LC chromatogram for model compound 1.

The chromatogram in Figure 22 successfully shows a peak in the LC spectrum for the starting material (model compound 1), suggesting that model compound 1 was present in each sample but the mass analyser could not detect the sample effectively. The chromatogram exhibited a high level of noise and overlapping peaks, which hindered the accurate identification and quantification of the compounds present. As can be seen in Figures 19 to 22, LCMS results were poor for the oxidised compounds, possibly indicating poor ionisation of the products.

Atmospheric pressure chemical ionisation (APCI) was used instead to determine whether a different ionisation source could ionise model compound 1 and its oxidation products in order to study the oxidation process in detail.

In the 72 h oxidised sample, it was found that there was a significant difference between the ionisation techniques, APCI-LC was able to successfully ionise the oxidised sample, whereas the standalone HPLC instrument first used was not able to. The oxidised sample (Figure 23) shows more peaks present for model compound 1 at t=0 in comparison to LC-MS; this is likely due to the more sensitive APCI-LC. The majority of the peaks that were present in model compound 1 at t=0 are also present in the oxidised sample at t=+72 h, suggesting the starting material (i.e. model compound 1) is still present as expected. Some peaks have stayed the same in both of the chromatograms, such as the peaks at 9.82, 11.46, 15.11, 16.07, 17.81, and 18.91 min. Figure 23 shows a peak at 20.35 min, but only in the oxidised sample at t=+72 h.

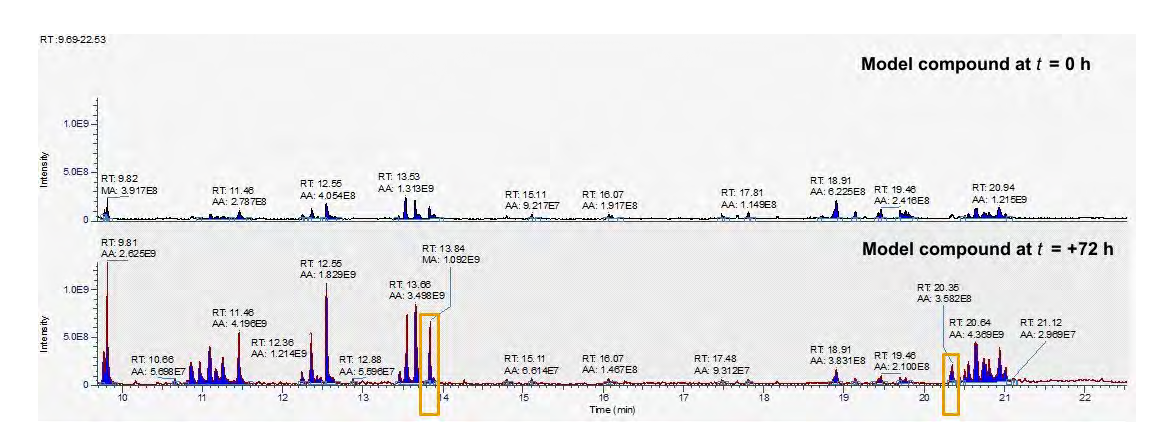


Figure 23: APCI chromatogram of model compound 1 (top) against the 72 h oxidised sample (bottom) with 5 wt% cobalt (II) stearate.

This data is consistent with the ¹H NMR data in suggesting that some degree of oxidation has occurred. The results imply that ionisation of model compound 1 was possible with APCI, although the chromatogram was quite crowded implying potentially poor signal to noise. The molecular ion was also visible using the APCI ionisation method, with chemical formulas of the oxidised species displayed in Table 1.

Table 1: APCI data showing the retention times for peaks in Figure 23

RT	Molecular ion m/z	Chemical ionisation confirmation?	Molecular formula
12.3	152.0	YES	$\mathrm{C_8H_8O_3}$
12.4	154.1	YES	$\mathrm{C_8H_{10}O_3}$
12.6	152.0	YES	$C_8H_8O_3$
13.5	156.1	YES	$\mathrm{C_8H_{12}O_3}$
13.7	154.1	YES	$\mathrm{C_8H_{10}O_3}$
13.8	154.1	YES	$\mathrm{C_8H_{10}O_3}$
14.3	129.0	no peak	$C_6H_9O_3$

At 14.26 min, a new peak was observed with a molecular ion m/z of 129.05, which could have a molecular formula of $C_6H_9O_3$, $C_6H_9O_2$, or $C_6H_9O_4$. All of these formulae correspond to hydroxyl-epoxide, peroxide, a ketone or aldehyde, and a peroxyacid, respectively, which are reasonably consistent with the expected oxidation products of the model alkenes. However, given that oxidation of conjugated dienes is commonly associated with epoxides, hydroxylated products, and bond cleavage, it is likely that the molecular ion m/z of 129.05 corresponds to an oxidised epoxy-alcohol or ketone derivative. It can also be depicted from the data that the peaks at 14.26 and 20.35 min elute later, suggesting increased polarity due to the incorporation of oxygen. This data is at best suggestive rather than conclusive, however, given the nature of the LC-APCI-MS chromatogram.

3.2 Model compound 2

A second synthesis was carried out (Scheme 2) due to the difficulties in the analysis with model compound 1. The structure of this new model compound 2 (Figure 24) was very similar to model compound 1, and it was synthesised in a similar way. They differed only in the presence of a benzoyl ester in place of the acetate. This was achieved by using benzoyl chloride in the synthesis in place of acetyl chloride. It was predicted that the introduction of a more polarisable aromatic functionality (via benzene) would improve the ionisation of the compound in LC-MS and could be used as the basis for subsequent model compounds based on functionalised benzoyl esters (for example, incorporating amines or other easily ionisable groups) if further improvements to ionisation were needed, whilst also adding aromaticity which is notably present in the real Amosorb® system incorporating PET. The ¹H NMR of model compound 2 is presented in Figure 24. After the successful synthesis of this model compound with a yield of 74%, oxidation tests were run the same way as the previous method, using room-temperature exposure to dry air.

Scheme 2: Reaction scheme for the synthesis of model compound 2.

3.2.1 Oxidation of model compound 2

A one-week exposure sample with 5 wt% cobalt (II) stearate was set up with model compound 2, this was chosen as an initial experiment to ensure a reasonable degree of oxidation in the hope that the oxidised products would be more easily analysed than those from model compound 1. In the course of this analysis

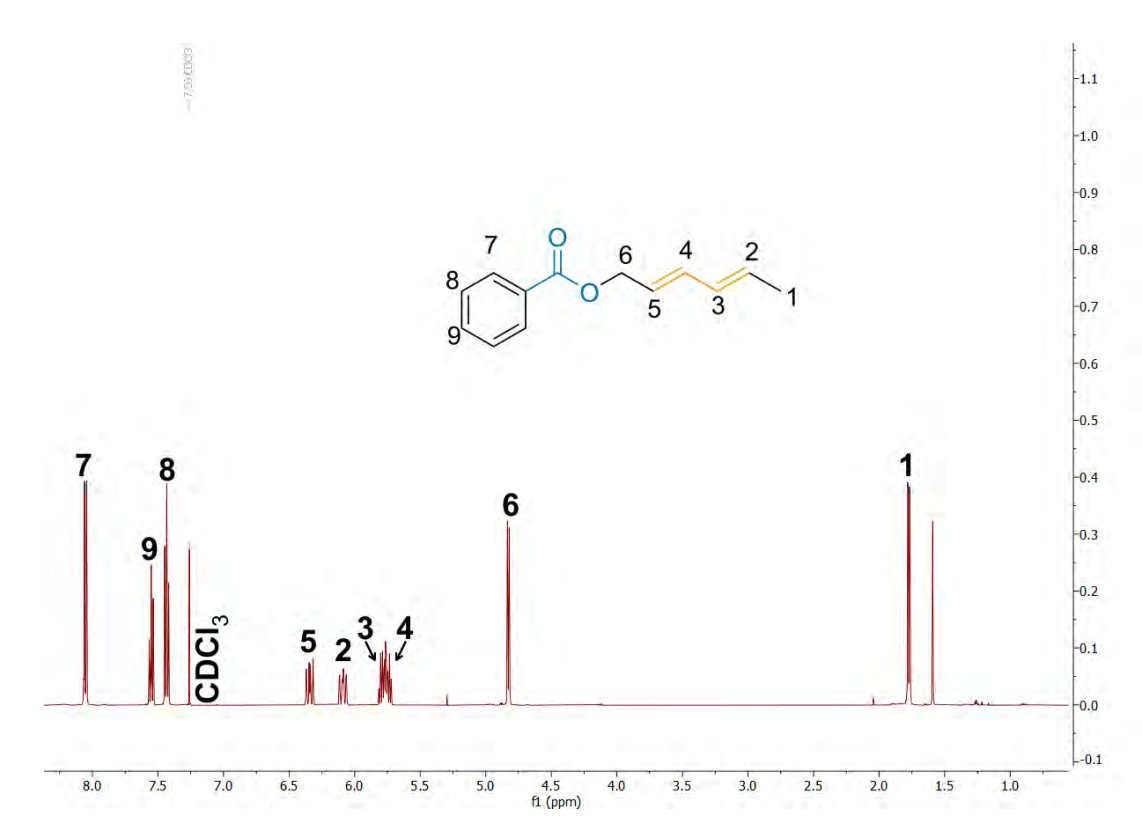


Figure 24: ¹H NMR spectrum of trans,trans-2,4-hexadienyl benzoate (model compound **2**).

was discovered that the broadening of peaks in the 1 H NMR could be a result of the presence of cobalt (II) stearate (Figure 25). Therefore, model compound 2 was filtered through silica to remove residual paramagnetic cobalt. A saturation recovery experiment was also performed to optimise quantification of any changes, and thus to calculate T_1 values to understand whether the presence of paramagnetic cobalt had an impact on the 1 H NMR data and obtain conditions where integration could be most accurate.

In addition, the ¹H NMR spectrum for the pure model compound **2** did not show unusual broad peaks, an issue that was encountered only with the cobalt (II) stearate samples (1 wt% and 5 wt%). Therefore, T_1 is calculated and present only for the samples with the paramagnetic cobalt.

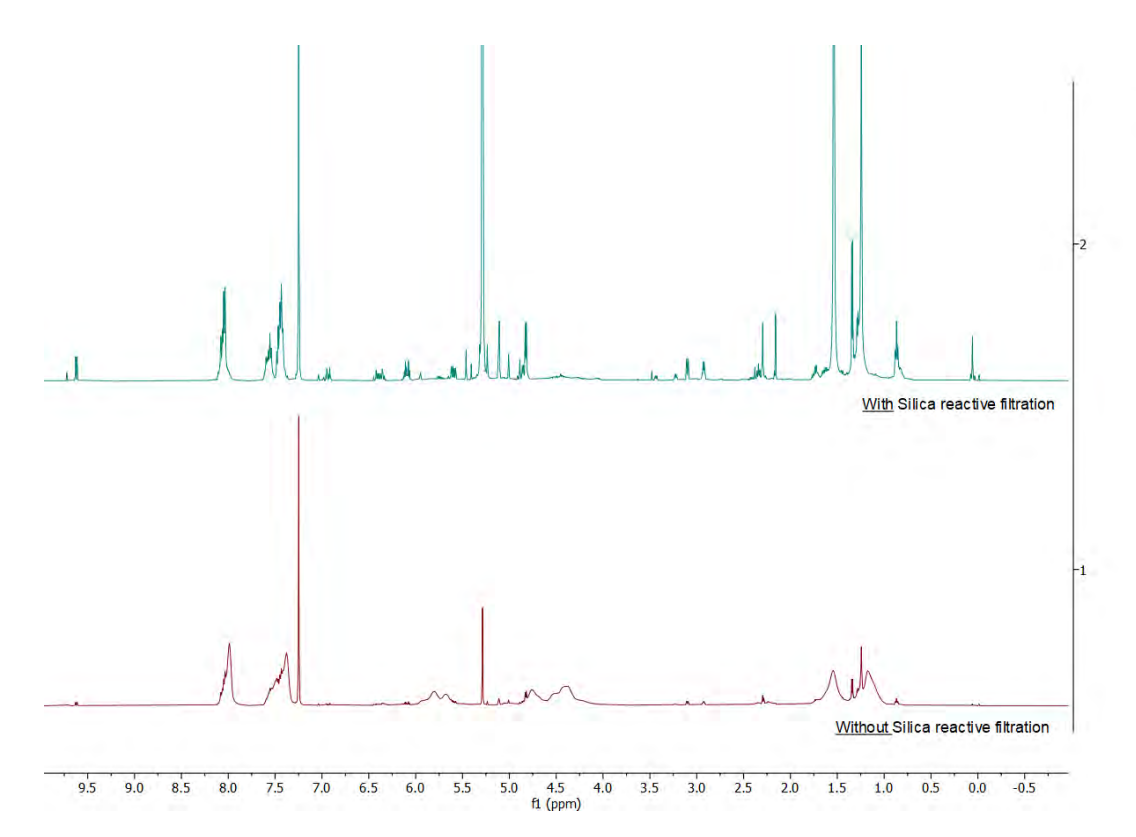


Figure 25: ¹H NMR of sample filtered with silica reactive filtration (top) and without (bottom) for 1-week sample with 5 wt% cobalt (II) stearate exposed to oxidation, showing peak broadening.

The presence of paramagnetic cobalt in a complex shortens T_1 relaxation times. The T_1 values when cobalt (II) stearate was present (Table 2) were lower compared to those when cobalt (II) stearate was not present (Table 3), because cobalt (II) stearate acts as a relaxation agent, enhancing the relaxation process. Conversely, T_1 values appeared larger when the cobalt (II) stearate was not present, as it lengthened the T_1 relaxation time (Table 3).

The implication of the presence of cobalt (II) stearate made it difficult to distinguish between closely spaced signals (Figure 25) so for future analysis, cobalt (II) stearate was removed from all oxidised samples using reactive filtration through a short plug of silica.

Table 2: Relaxation measurement values (T_1) for 1-week with 5 wt% cobalt (II) stearate that was not filtered via reactive silica filtration. Where there is a dash (-), T_1 could not be calculated.

Proton number	Integrals	T_1 (s)
7	8.206-7.801	2.43
8	7.647 - 7.472	_
9	7.491 - 7.280	_
4	6.521 – 6.282	10.46
3	6.147, 6.051	3.75
2 and 5	5.975, 5.536	1.47
6	4.847 – 4.805	1.29
1	1.775, 1.691	_

Table 3: Relaxation measurement values (T_1) for 1-week with 5 wt% cobalt stearate that was filtered via reactive silica filtration to remove residual paramagnetic cobalt.

Proton number	Integrals	T_1 (s)
7	8.148-8.002	4.28
8	7.644 - 7.523	3.83
9	7.582 - 7.400	3.56
4	6.497 – 6.326	5.57
3	6.169 – 5.954	3.64
2 and 5	5.676 – 5.516	3.07
6	4.859 – 4.805	2.08
1	1.604 – 1.493	5.59

For example, a T_1 value of 1.29 was achieved for structural group 6 (protons on the aromatic benzene ring) in the non-filtered sample, compared to the same structural group in the filtered sample, which had a T_1 value of 2.08.

The peaks were much more easily identifiable after the removal of the paramagnetic cobalt (II) stearate, and it was discovered that potentially product 4 (Figure 26) may have formed upon oxidation. It was concluded that there was the presence of an epoxide (Figure 26) and a small amount of aldehyde formed upon oxidation for model compound 2. Though compound 4 was not isolated purely despite several attempts to isolate it, there were significant peaks that could still be assigned. For the presence of epoxide, Table 4 presents the data.

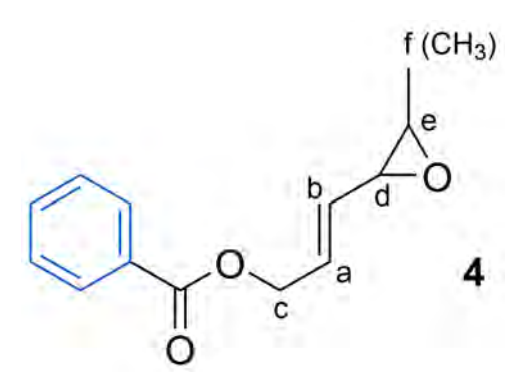


Figure 26: Structure of oxidised model compound 2, showing an epoxide ring (4).

Table 4: Analysis of ¹H NMR spectrum achieved for the 1-week oxidation of model compound **2** with cobalt (II) stearate filtered out.

Signal	δ / ppm	Multiplicity	J-coupling / Hz
На	6.09	dt	$0.6 \ / \ 5.88 \ / \ 15.50$
Hb	5.59	ddt	$1.47\ /\ 7.60\ /\ 15.66$
Hc	4.82	dd	$1.53 \ / \ 5.94$
Hd	3.10	dd	$2.12 \ / \ 7.66$
Не	2.93	dq	$2.13 \ / \ 5.20$
Hf	1.34	d	5.17

The peak H_a at 6.09 ppm is of a dt multiplicity that integrates to 0.24 protons and has the adjacent peaks, H_c and H_d in compound 4 (Figure 26). The chemical shift indicates that the peak (H_a) corresponds to the alkene C-H bond. The next peak H_b at 5.59 ppm is of a ddt multiplicity and integrates to 0.22 protons. The integrations are relative to the benzene group in compound 4 (Figure 26). Both of these peaks correspond to the protons on the alkene chain and, therefore, appear further downfield due to the deshielding effects of the double bonds and the nearby electronegative oxygen atom.

The peak H_c at 4.82 ppm is of a dd multiplicity that integrates to 0.50 protons and corresponds to the methylene group (-CH₂) in compound 4 (Figure 26). The CH₂ was previously a doublet, so it may indicate that oxidation caused additional coupling interactions. This group appears further upfield due to the shielding effects of the electronegative oxygen. The protons on H_d and H_e, which previously corresponded to a double bond, have now been transformed into an epoxide ring upon oxidation, evident in Figure 27.

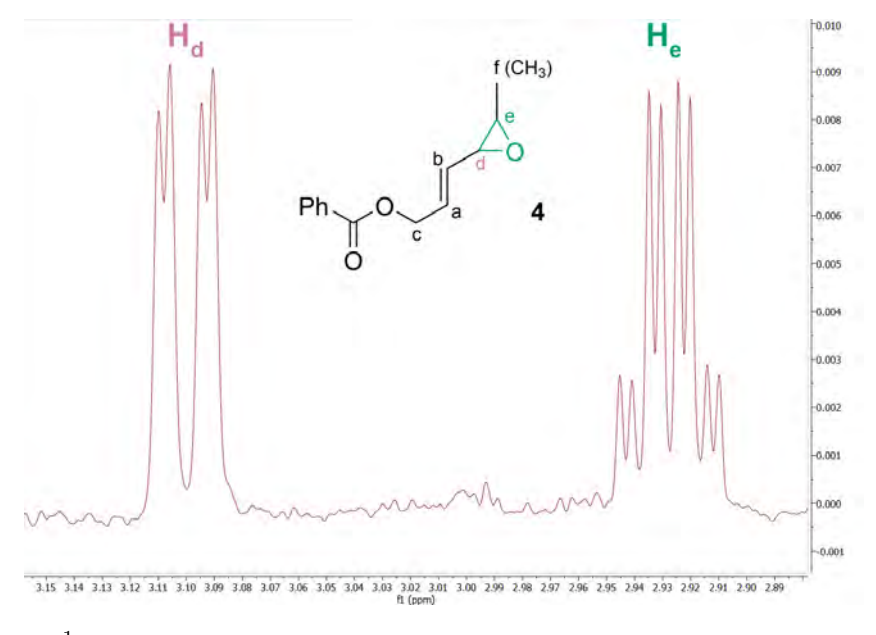
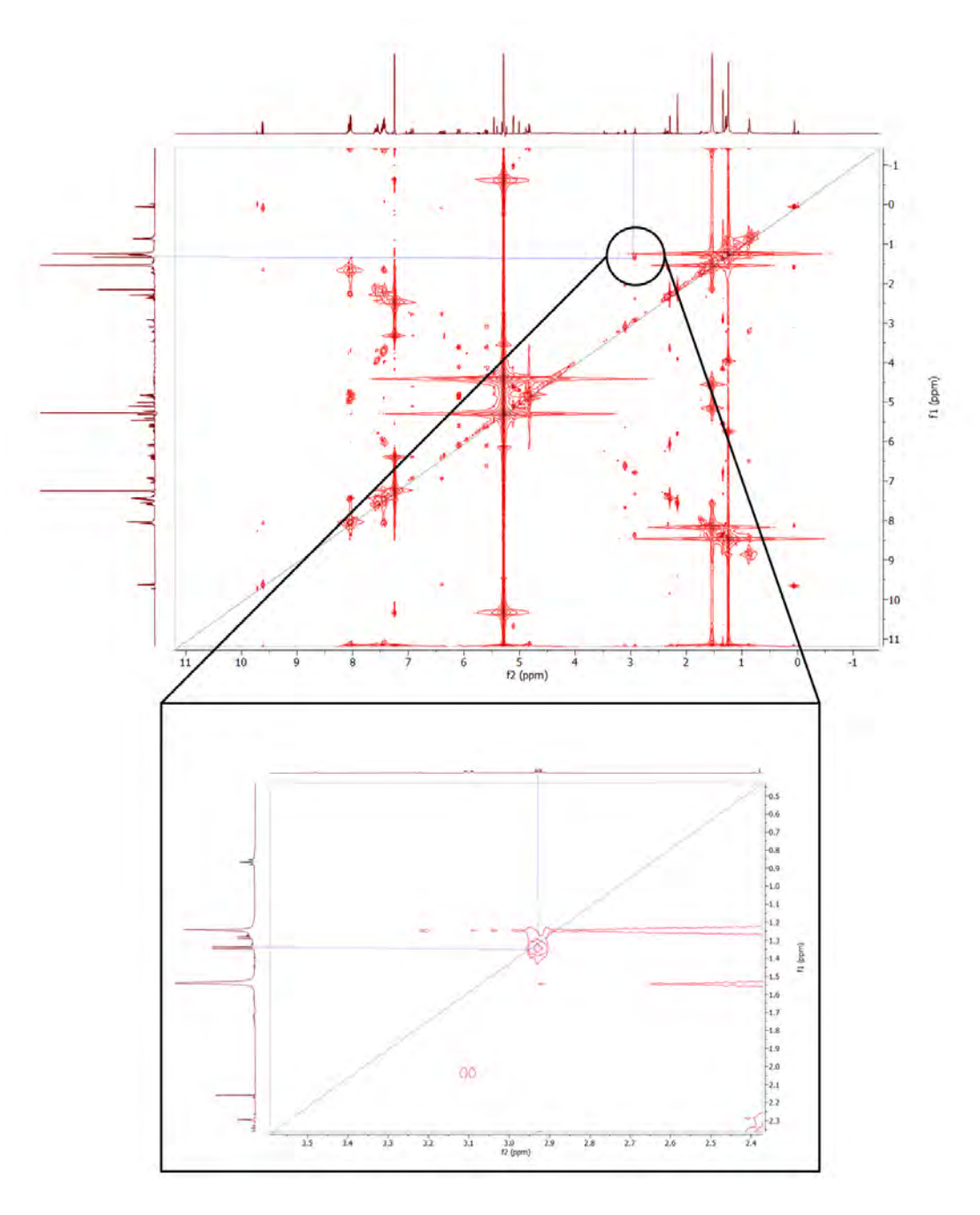


Figure 27: 1 H NMR spectrum for the 1-week oxidised sample showing the peaks for protons $H_{\rm d}$ (pink) and $H_{\rm e}$ (green), diagnostic of an epoxide. The full figure is available as Figure A10.

The peak H_d at 3.10 ppm is of a dd multiplicity and the next peak is H_e at 2.93 ppm, a dq, where both integrate to 0.22 protons. Correlation spectroscopy (COSY) showed a coupling between H_e and H_f, evident in Figure 28. This, in addition to the ¹H NMR spectra, confirms the presence of the epoxide at those positions in compound 4 (Figure 26). The epoxide protons H_d and H_e (3.10 ppm and 2.93 ppm respectively) are present in the literature. Although ¹³C NMR data was not collected in this study, the ¹³C NMR data in the literature specified the signals to be at 58.9 ppm and 56.5 ppm for the carbons in the epoxide.⁷²

The final peak H_f at 1.34 ppm is a doublet that integrates to 0.94 protons, corresponding to the methyl group on compound 4 (Figure 26). This peak has changed chemical shift from being at 1.75 ppm in the starting material (Figure 24) to now being 1.34 ppm. This could indicate that the oxidation process might have increased electron density around the methyl group, leading to greater shielding of the protons.⁷⁴ The integrals achieved for protons H_a to H_f are non-normalised; however, upon normalisation, they give the ratios 1:1:2:1:1:3.

As shown in Figure 29, a small set of peaks appeared in the region 9.60 - 9.75 ppm. The doublet at 9.62 ppm integrates to 0.14 protons and appears to suggest the formation of aldehyde(s). The singlet is a lot more difficult to assign as the proton is not attached to a carbon with one H (proton) attached. The most likely is for the formation of an aldehyde as another alternative could be a formate ester, but these appear usually at 8.5 ppm which isn't seen here. The exact structure of these products is not clear, but given the lack of evidence for free carboxylic acid may result from β -scission of peroxides formed on the alkenes, which is known in the literature.⁷⁵



 $\label{eq:Figure 28: COSY spectrum of 1-week oxidised sample with 5 wt\% cobalt (II) stearate. Inset: zoomed region showing coupling between H_d and H_e.}$

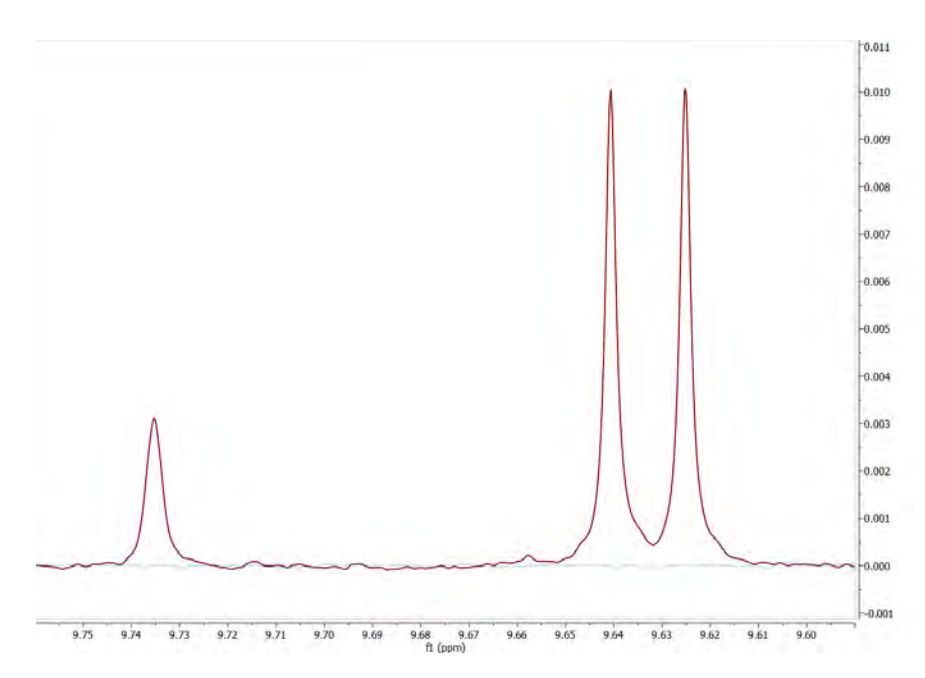


Figure 29: ¹H NMR spectrum of the 1-week oxidised sample (with 5 wt% cobalt (II) stearate) showing a peak at 9.62 ppm consistent with formation of an aldehyde group in model compound **2**. The full figure is available as Figure A10.

The peaks above 9 ppm might be indicative of aldehydes but these were not visible in the ¹³C NMR data (Figure A11) so it is inconclusive.

The LC-MS results of the oxidation of model compound **2** showed no ionisation, similar to the results of model compound **1**. This lack of ionisation was deduced by the very poor peak separation in the chromatogram (Figure 30), which obscured potential diagnostic peaks for epoxides and aldehydes.

Finally, model compound $\mathbf{2}$ was ionisable on GC, with a molecular ion peak of m/z 202.1 (highlighted by the circle) present on the mass spectrum (Figure 31). This confirmed the successful ionisation of model compound $\mathbf{2}$, which was not possible with model compound $\mathbf{1}$.

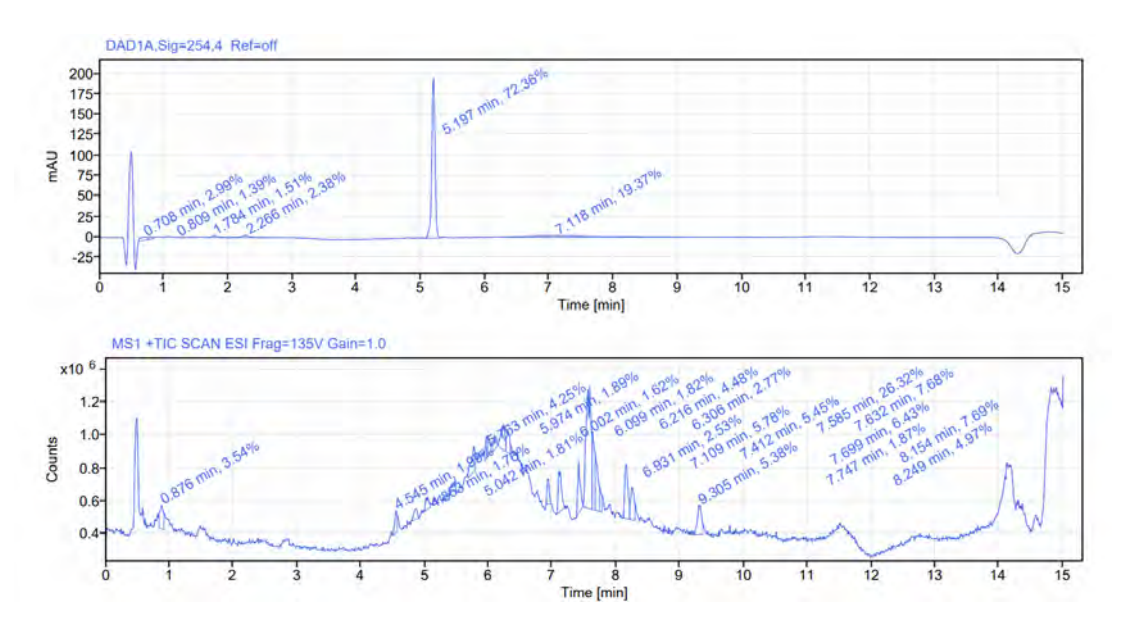


Figure 30: LC of 48 h oxidised sample with 5 wt% cobalt (II) stearate showing DAD (top) and LC chromatogram (bottom).

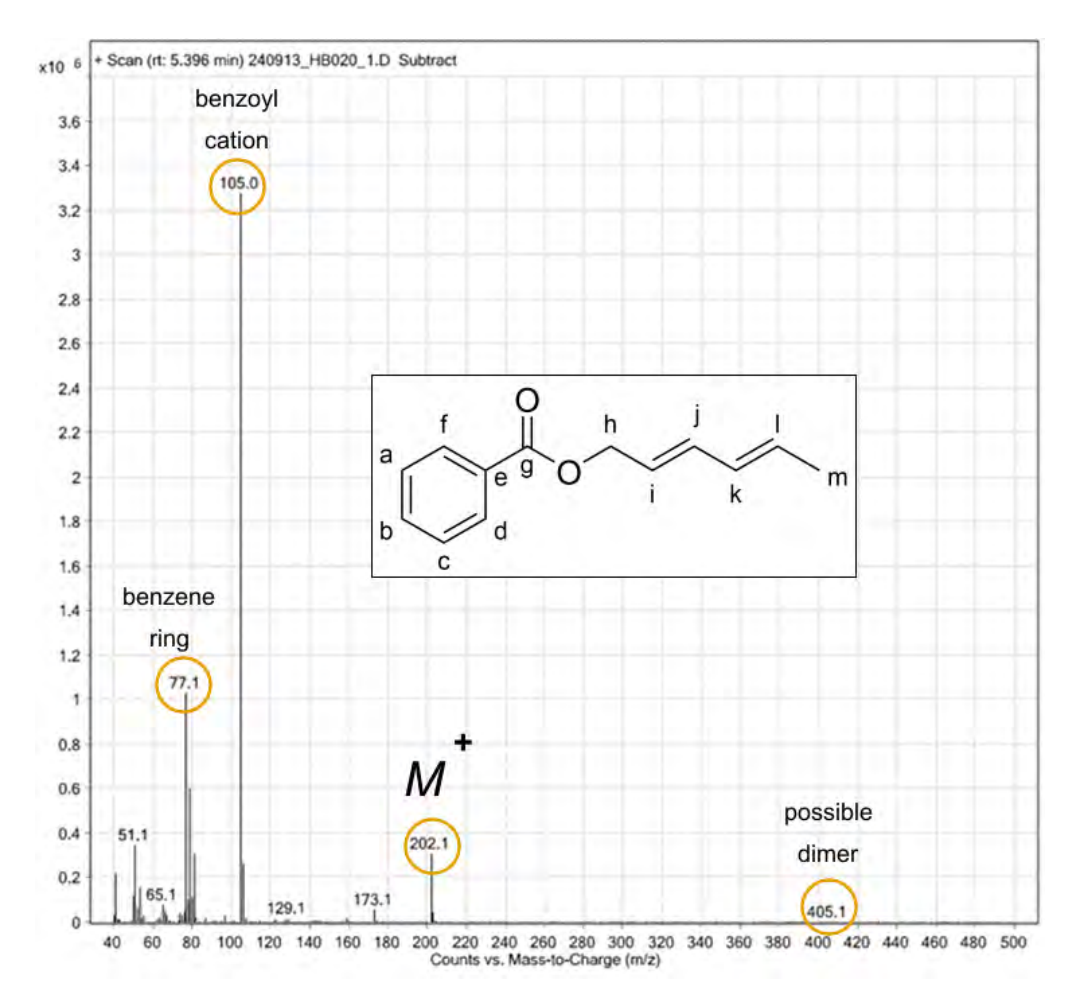


Figure 31: GC mass spectrum of model compound **2**. See chromatogram in Figure A12.

The peak at t=7.7 min was present in all blanks (Figure A13), so it can be regarded as background noise. However, the peak at a t=5.4 min was only present in the 5 wt% oxidised sample (Figure 32). There is a diagnostic pair of peaks at m/z 105 and m/z 77. It is assumed that the m/z 105.0 is M-1 from benzaldehyde with a molecular weight $(M_{\rm w})$ of 106 g/mol. This signifies a loss of a hydrogen atom, hence m/z 105.0 could be a peak for an aldehyde cleavage.

The m/z 77, on the other hand, is the phenyl cation from the cleavage of the bond between the benzene ring and the carbonyl group. The peak characteristic of an epoxide which should appear at m/z 129 may be present but obscured by more intense peaks in the GC mass spectrum; the peak is present for the 48 h exposure at 0, 1 and 5 wt% cobalt (II) stearate (Figures A14 to A16). The m/z 135.1 peak is likely to be a structural rearrangement, possibly involving the opening of the benzene ring. The rest of the peaks, m/z 281.0, 327.0, 404.9, and 478.9, are due to column bleeding from the GC column, especially the 281.0 and 327.0, which are diagnostic of siloxane peaks. Therefore, the GC confirms the presence of a phenyl ester. However, further analysis and comparison are necessary to confirm the exact nature of the oxidation of model compound 2.

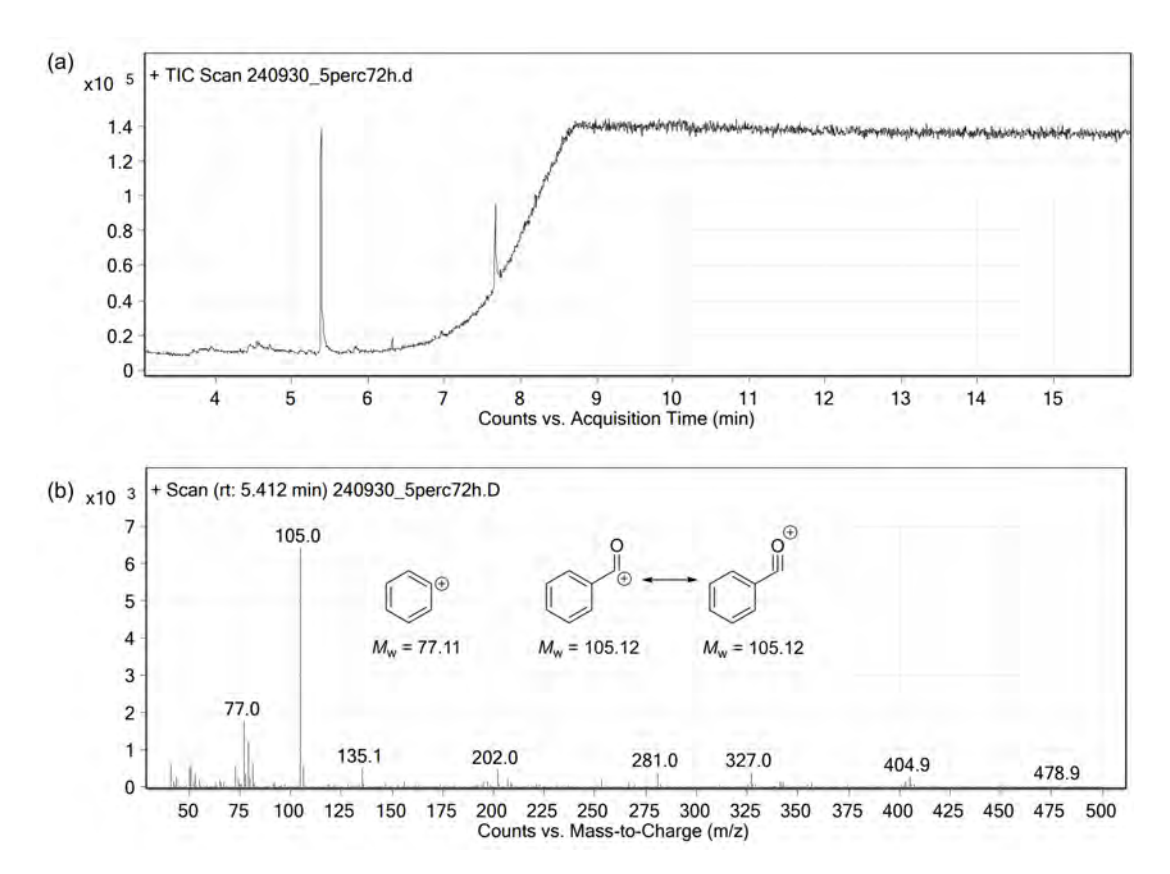


Figure 32: A GC chromatogram showing (a) an oxidised sample of 5 wt% cobalt (II) stearate for 72 h reaction. A mass spectrum (b) from part (a). The data for 0 and 1 wt% is available in Figures A17 to A18.

4 Conclusions

Two model compounds were prepared as small molecular simplified analogues of Amosorb®, and both oxidised in the presence of cobalt (II) stearate on exposure to dry air. The oxidation products proved challenging to characterise, with the acetate ester model compound 1 in particular being very intractable for analysis by both GC and LCMS with either electrospray or chemical ionisation. Detailed NMR analysis, following the removal of cobalt to improve the resolution of the spectra, revealed that epoxide products were being produced in both cases, though the evidence for this was more convincing for the benzoate ester model compound 2. Some evidence was also observed in the NMR suggesting the for-

mation of aldehydes, possibly through a β -scission mechanism. The GC and LC data of the oxidised sample with model compound **2** also proved challenging in characterising the oxidised product(s).

5 Future Work

Future efforts to understand the oxidation chemistry of Amosorb® via the use of model compounds might focus on two main areas:

Improvement of analysability: Although the benzoate ester model compound 2 was somewhat successfully analysed by ¹H NMR, the reluctance of both compounds to ionise hampered efforts to characterise and quantify the products of oxidation using LC or GC mass spectrometry. Therefore, a logical next step would be to substitute the simple benzoyl chloride for a more ionisable species such as the p-amino benzoyl chloride. However, care must be taken to ensure that the amine does not participate in side reactions or undergo oxidation itself, which could complicate spectral interpretation. In theory, this should allow more straightforward quantification of oxidation products by LCMS, greatly simplifying the process of understanding this oxidation.

Stoichiometric oxidation: It may prove valuable to deliberately prepare and isolate samples of oxidised products by, for example, oxidation with stoichiometric mCPBA (meta-chloroperbenzoic acid).⁷⁶ These might then be fully purified and characterised for use as both analytical standards to be compared to oxidation products observed from air-exposure of the primary model compounds and as models in their own right for investigations of the degradation (yellowing) of these oxidation products on storage or heating.

It can be reasonably anticipated that these two steps would rapidly permit a better understanding of the Amosorb® oxidation products and their subsequent degradation. If necessary, more sophisticated model compounds, perhaps containing PET oligomers, could be prepared to more closely mimic the Amosorb® formulation. It is also possible that forearmed with better knowledge of the likely products, it would be possible to analyse the oxidation products of Amosorb® itself.

Acknowledgements

Many thanks to my supervisory team, Dr Ian Ingram, Dr Ryan Mewis and Dr Ed Randviir for their support throughout the project as well as Patrick Brown (Avient Ltd) who advised from the industrial perspective. Thanks to the team at Avient™ for carrying out APCI analysis. Amosorb® is a registered trademark of ColorMatrix Holdings, Inc. Thanks also to the technical services team as well as the Analytical Core Facility for their assistance in instrumental analysis. A special thanks to Dr Emily Griffiths for continued moral support throughout the project.

Appendix

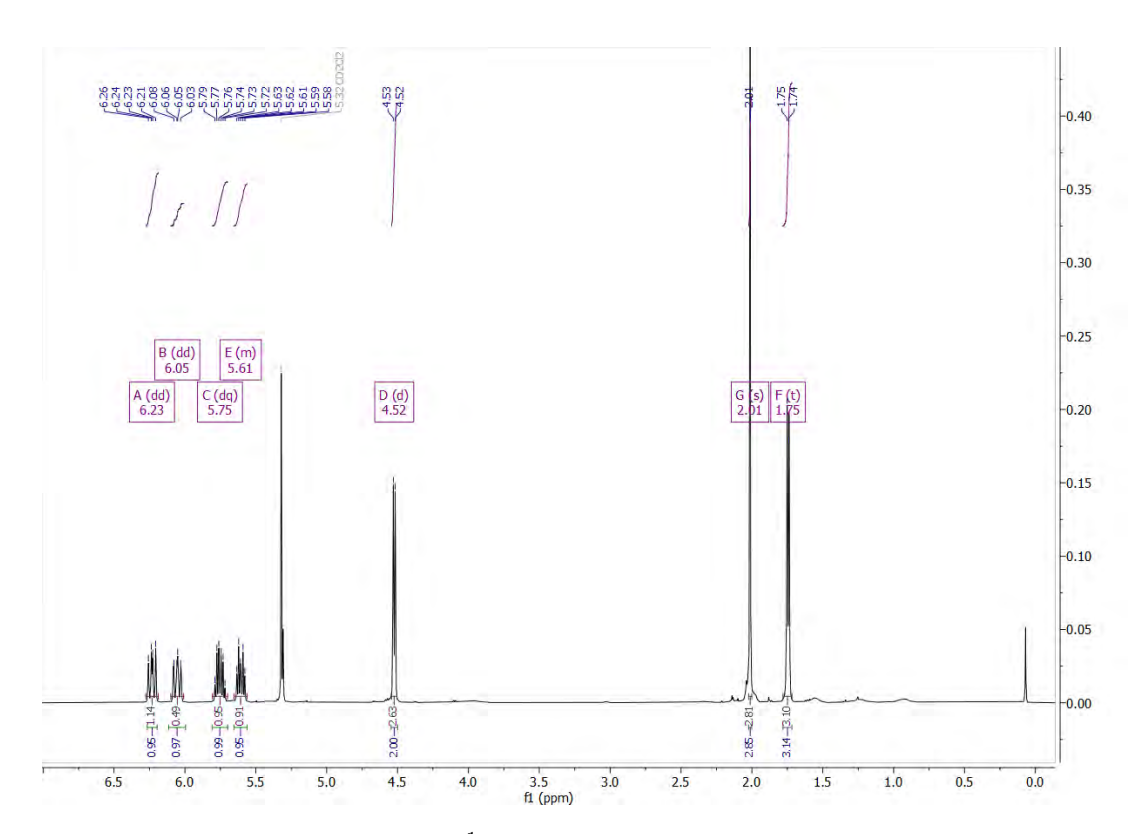


Figure A1: 1 H NMR of model compound 1.

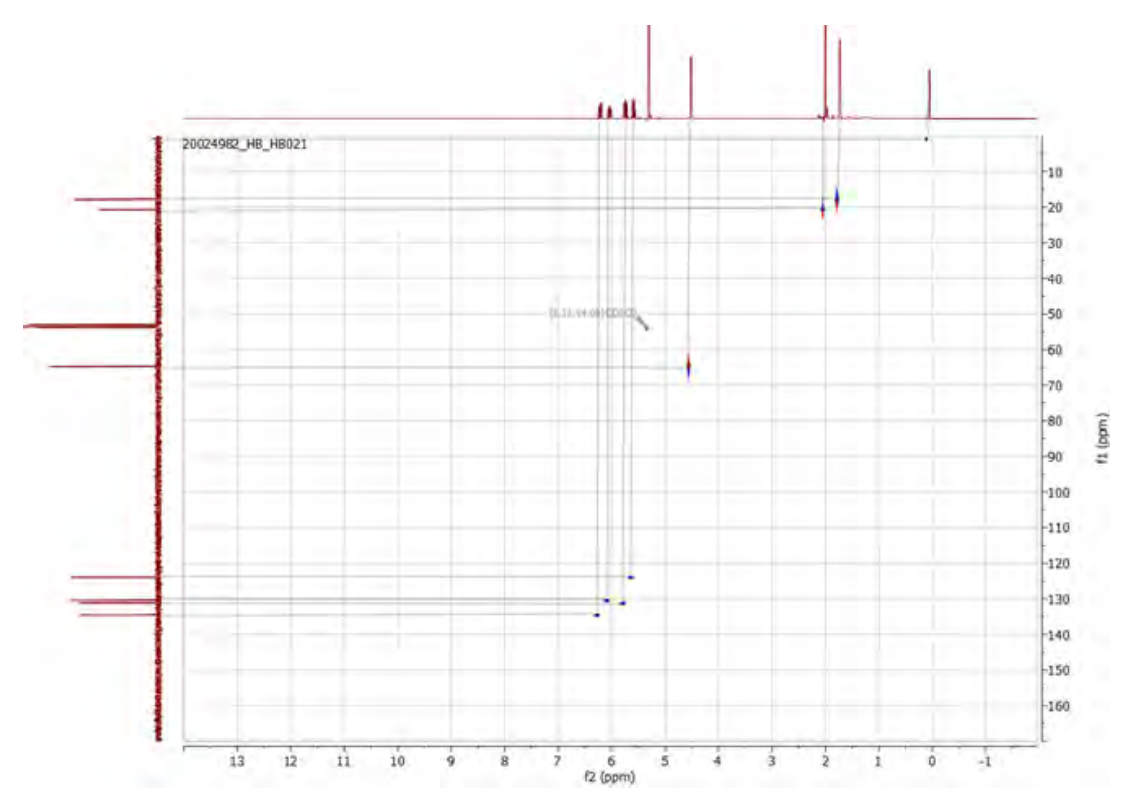


Figure A2: HSQC NMR of model compound 1 assigned using 13 C and 1 H NMR.

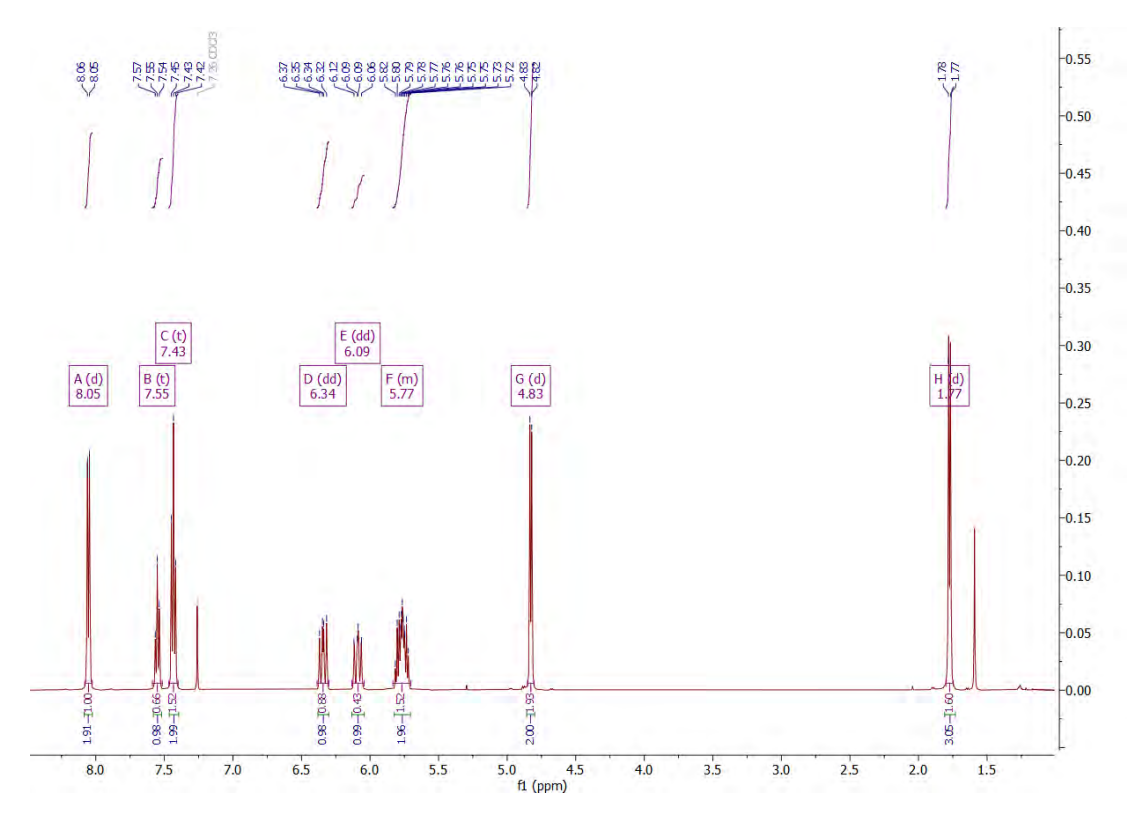


Figure A3: 1 H NMR of model compound 2.

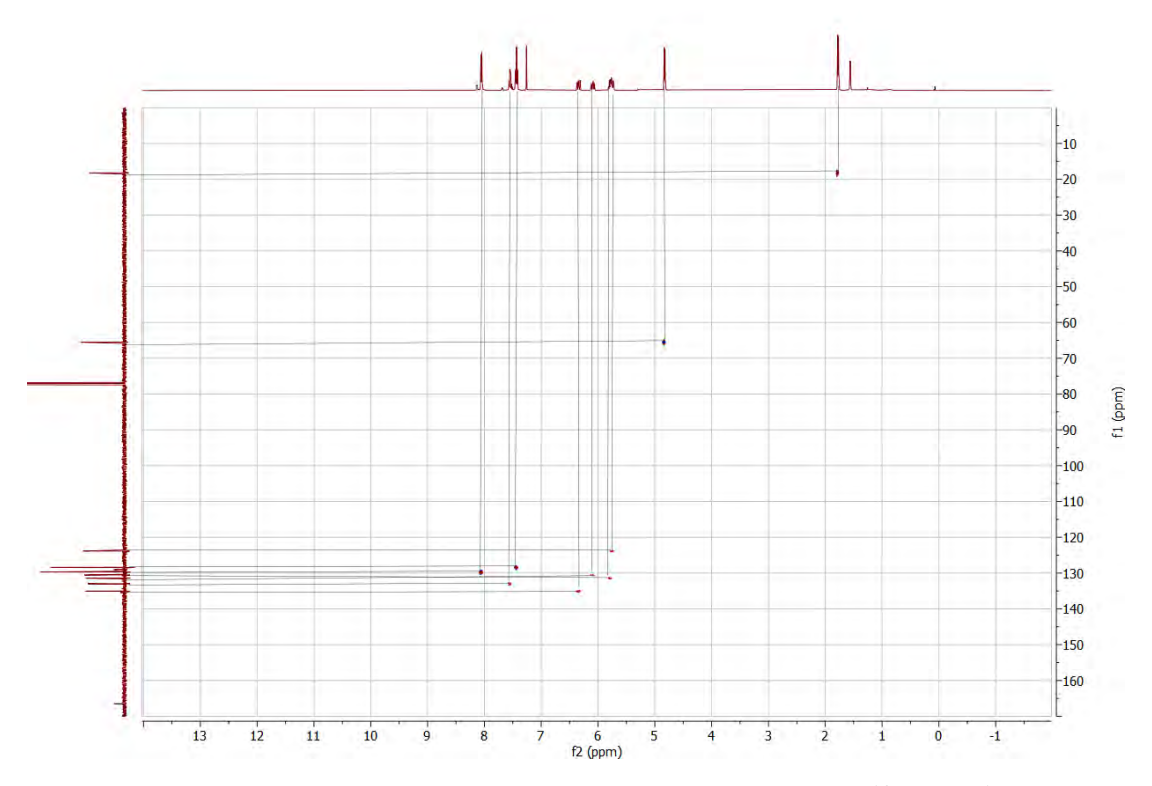


Figure A4: HSQC NMR of model compound 2 assigned using $^{13}\mathrm{C}$ and $^{1}\mathrm{H}$ NMR.

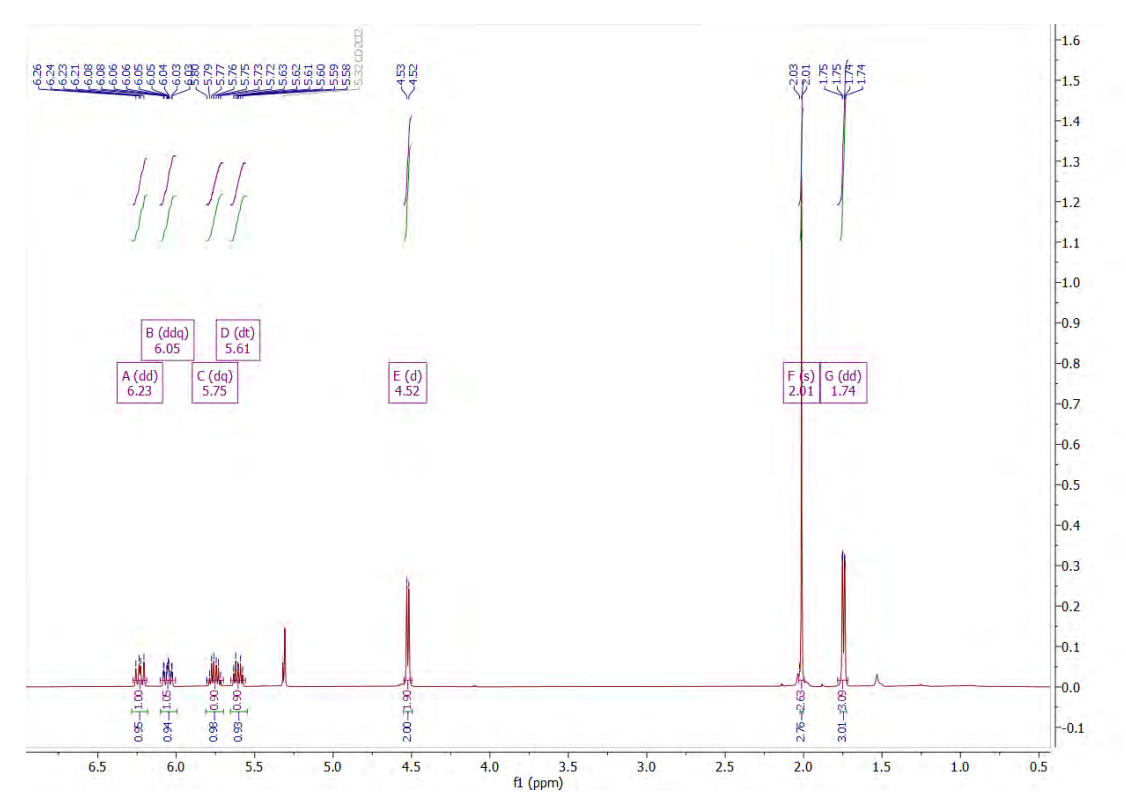


Figure A5: $^1{\rm H}$ NMR of an oxidised sample with 0 wt% cobalt (II) stearate at 72 h for model compound 1.

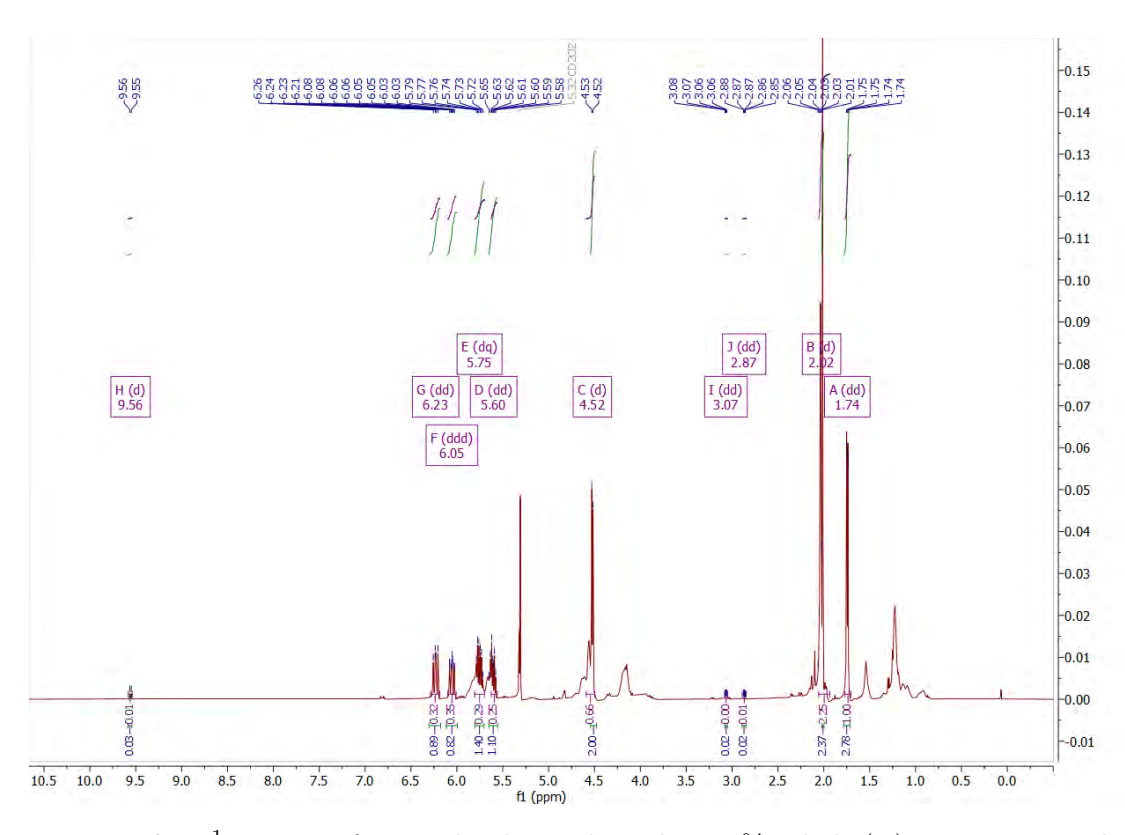


Figure A6: ¹H NMR of an oxidised sample with 1 wt% cobalt (II) stearate at 72 h for model compound **1**.

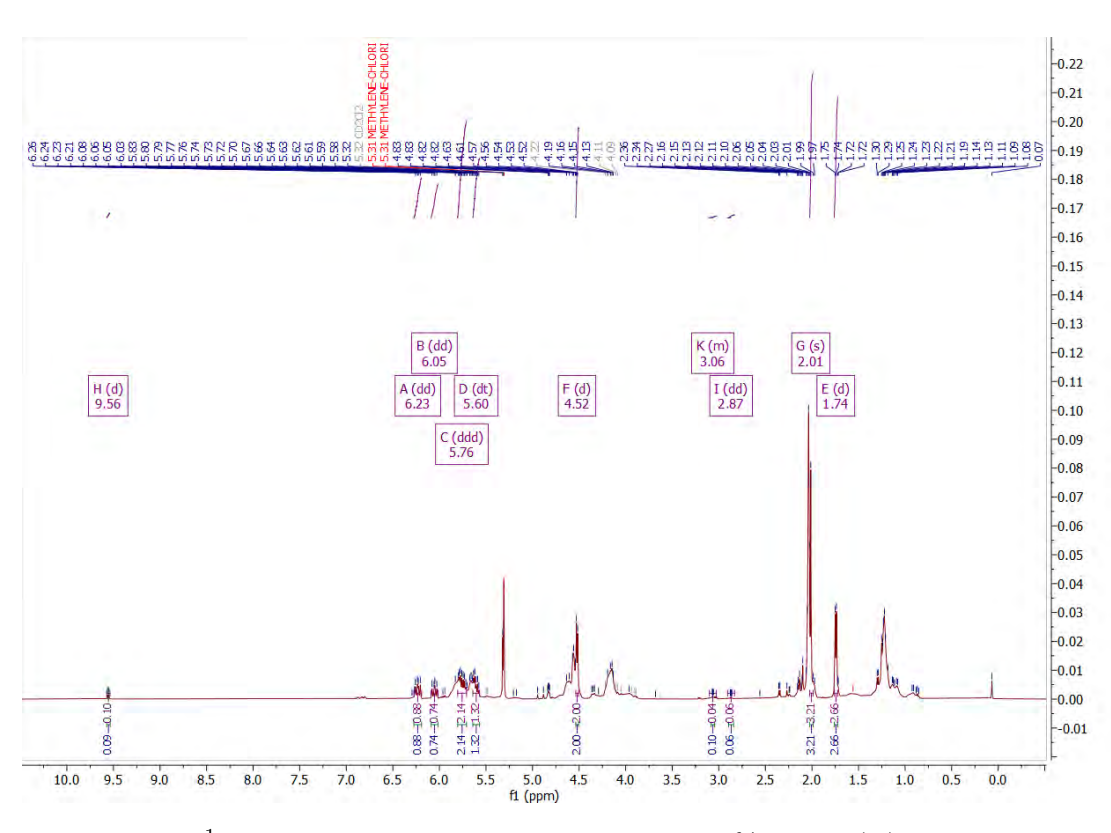


Figure A7: ¹H NMR of an oxidised sample with 5 wt% cobalt (II) stearate at 72 h for model compound **1**.

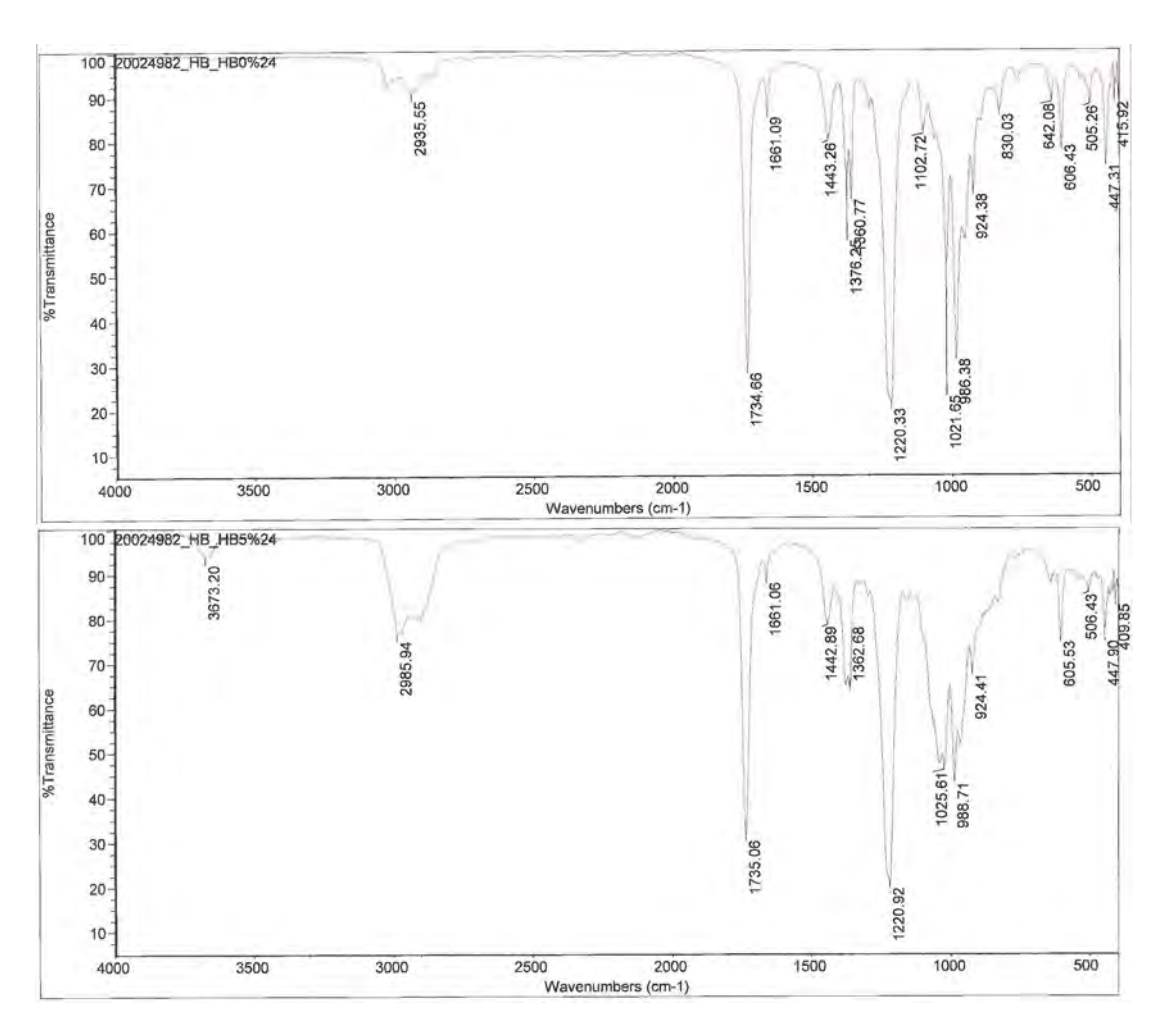


Figure A8: FTIR spectra of model compound $\bf 1$ with 0 (top) and 5 (bottom) wt% cobalt (II) stearate at 24 h exposure.

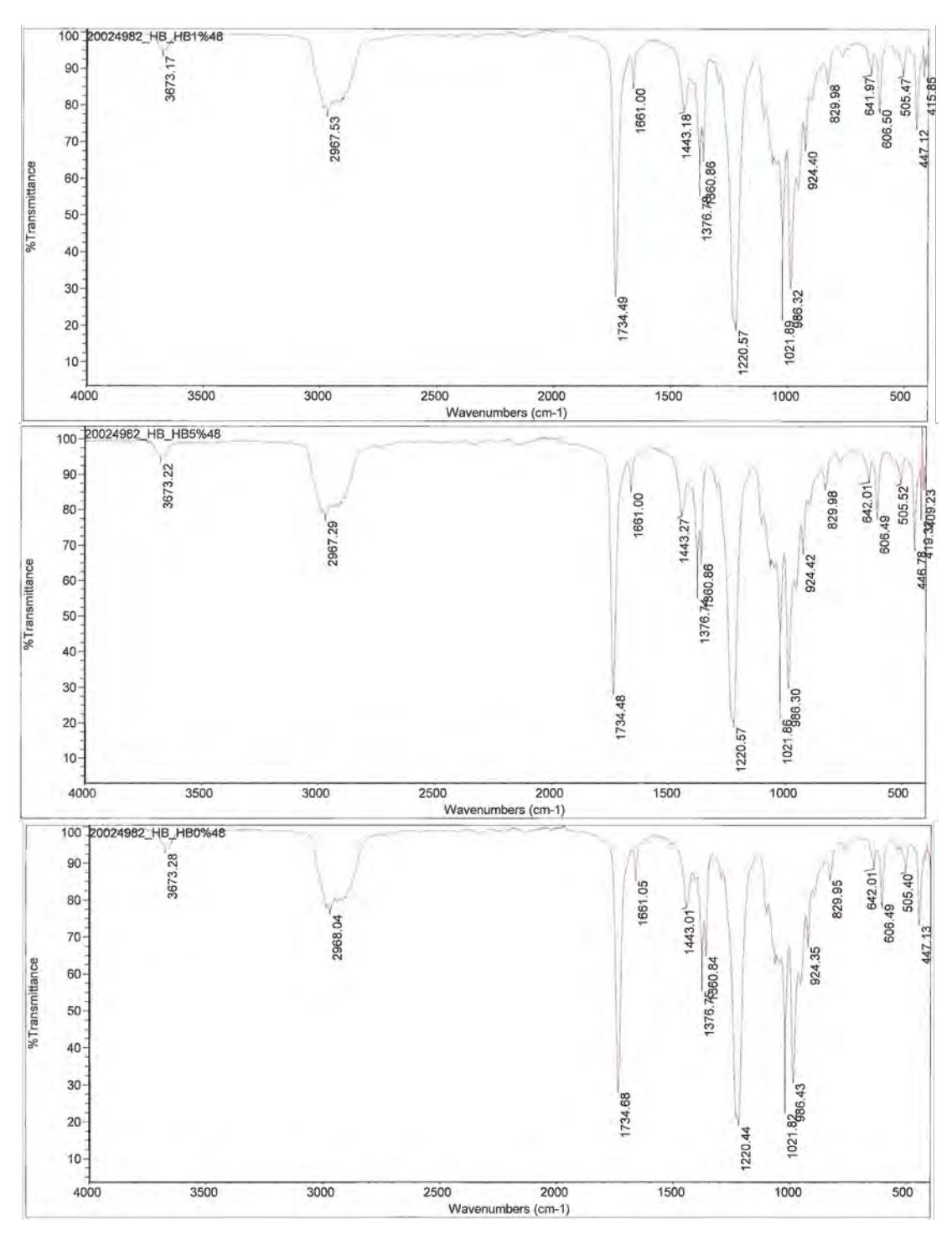


Figure A9: FTIR spectra of model compound **1** with 0 (top), 1 (middle) and 5 (bottom) wt% cobalt (II) stearate at 48 h exposure.

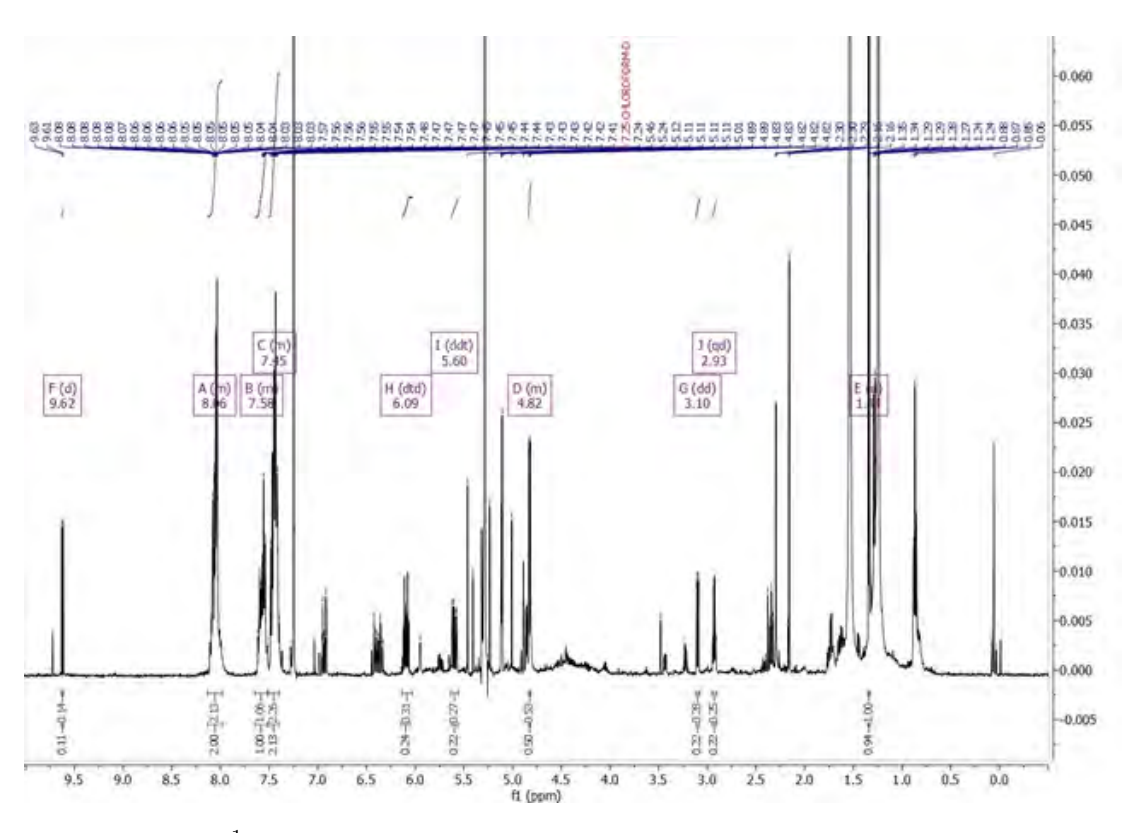


Figure A10: ¹H NMR of model compound **2** at 1-week oxidation exposure with 5 wt% cobalt (II) stearate that was silica filtered.

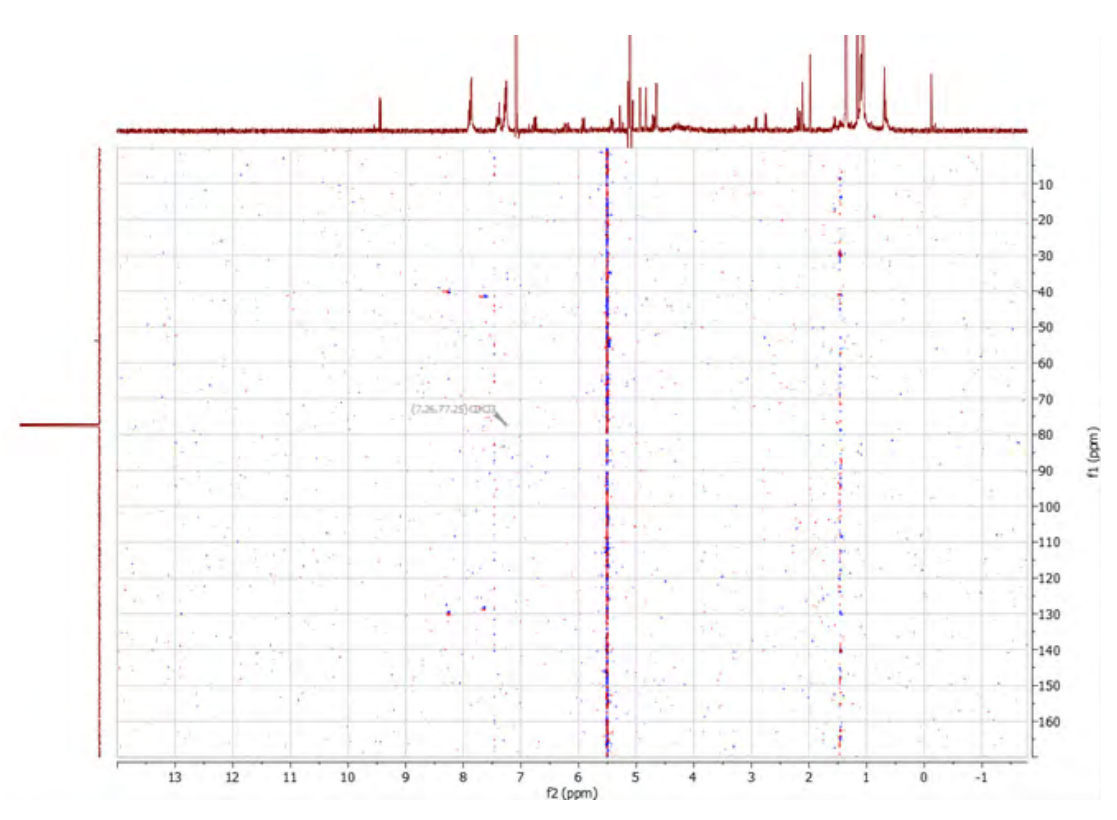


Figure A11: 13 C analysis via HMBC spectroscopy of model compound 2 for silica-filtered 5 wt% 1-week exposure sample.

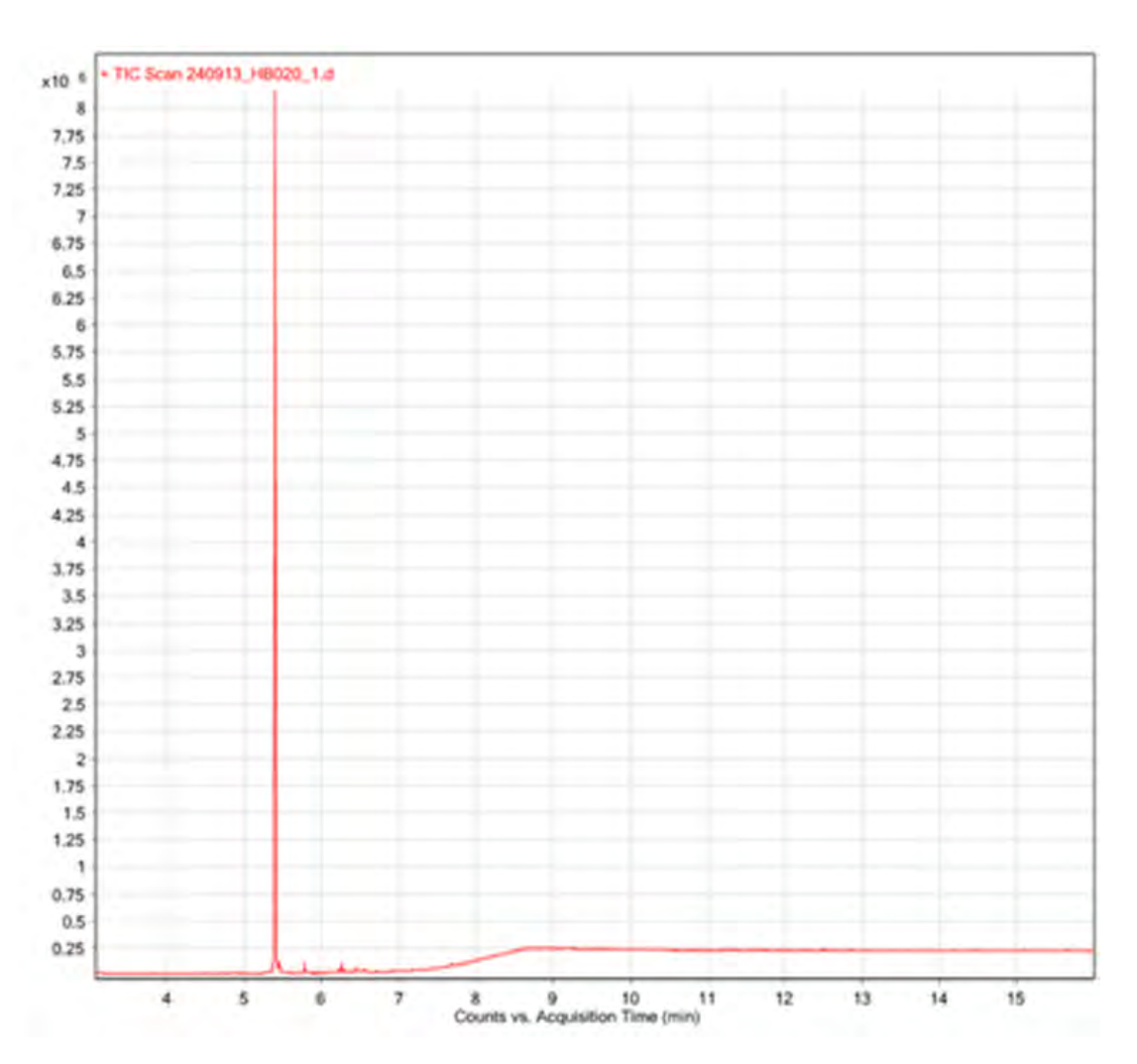


Figure A12: GC chromatogram of model compound 2.

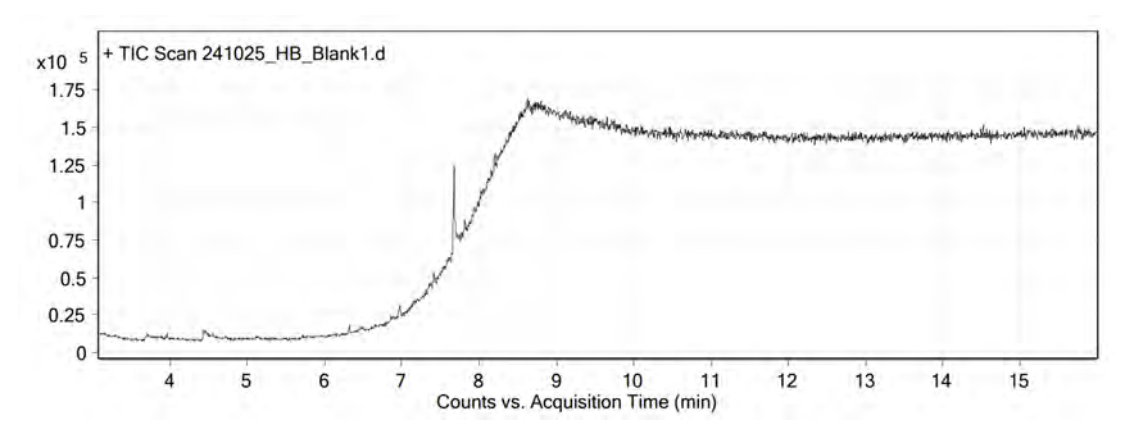


Figure A13: GC chromatogram of a blank for the GC-MS analysis of the 5 wt% cobalt (II) stearate for 72 h exposure for model compound **2**.

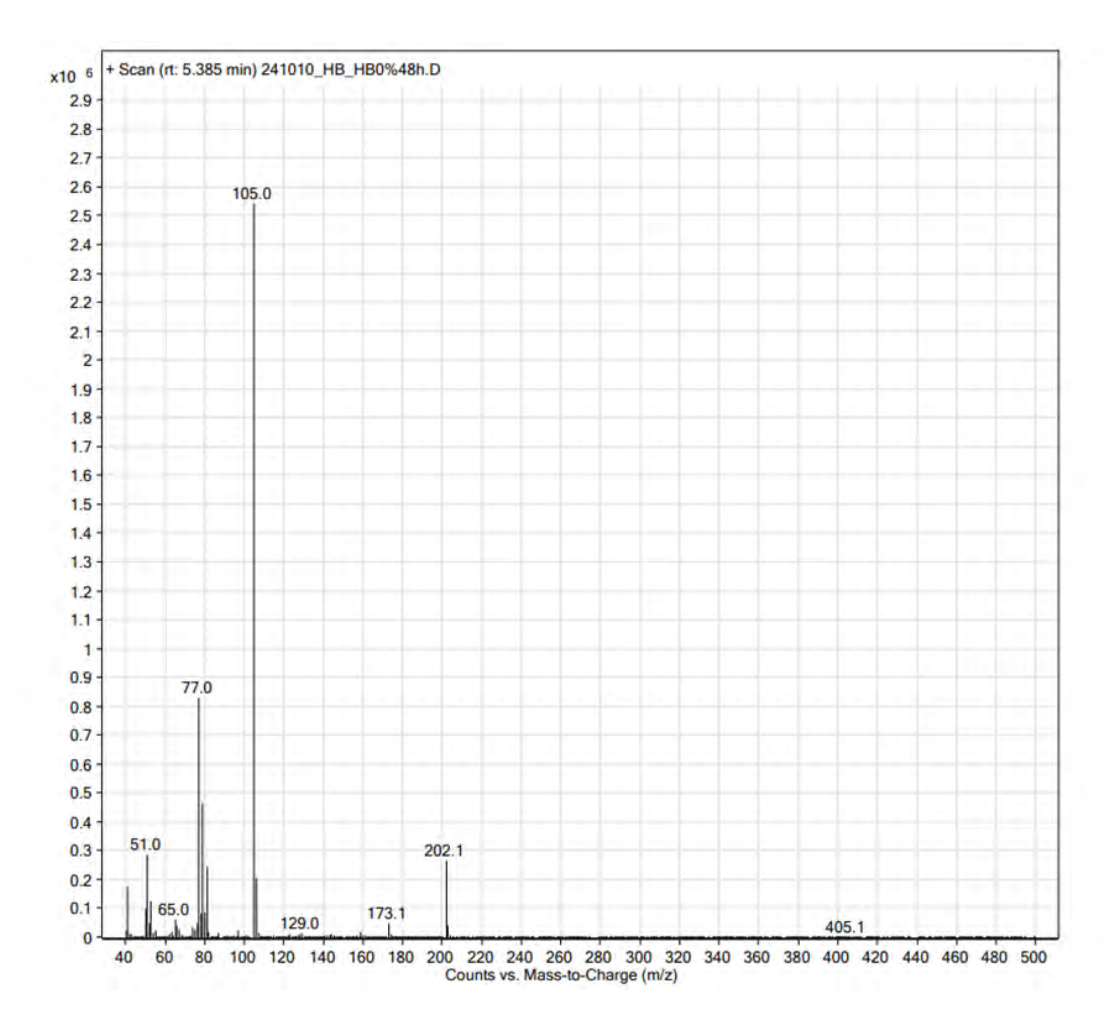


Figure A14: GC mass spectrum of 48 h oxidised sample with 0 wt% cobalt (II) stearate for model compound **2**.

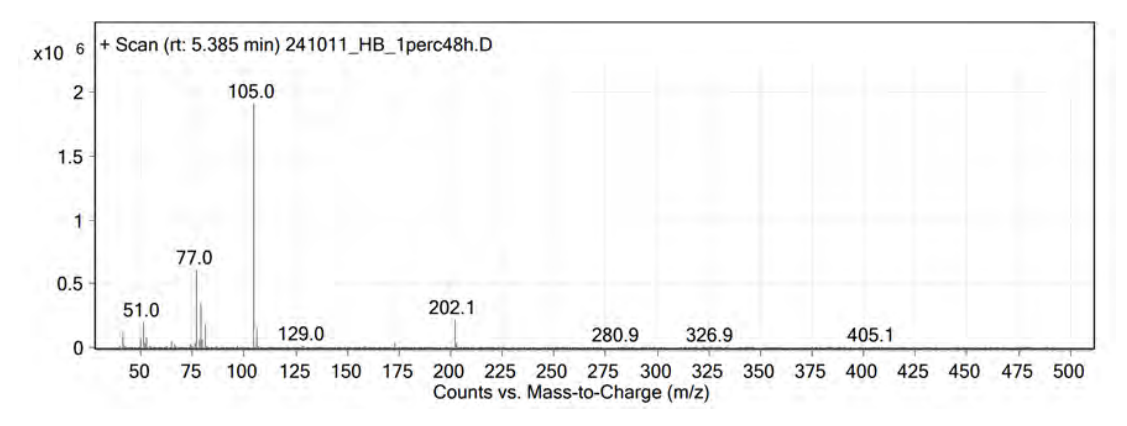


Figure A15: GC mass spectrum of 48 h oxidised sample with 1 wt% cobalt (II) stearate for model compound **2**.

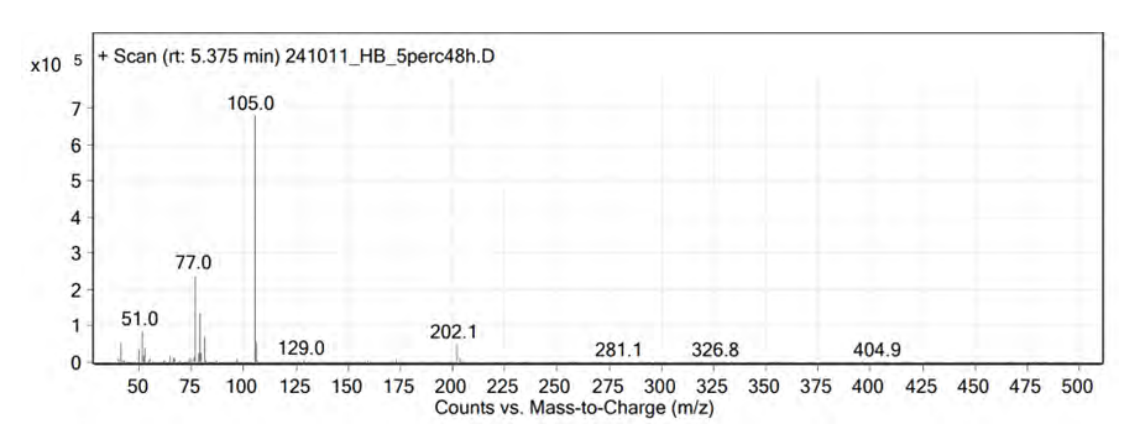


Figure A16: GC mass spectrum of 48 h oxidised sample with 5 wt% cobalt (II) stearate for model compound **2**.

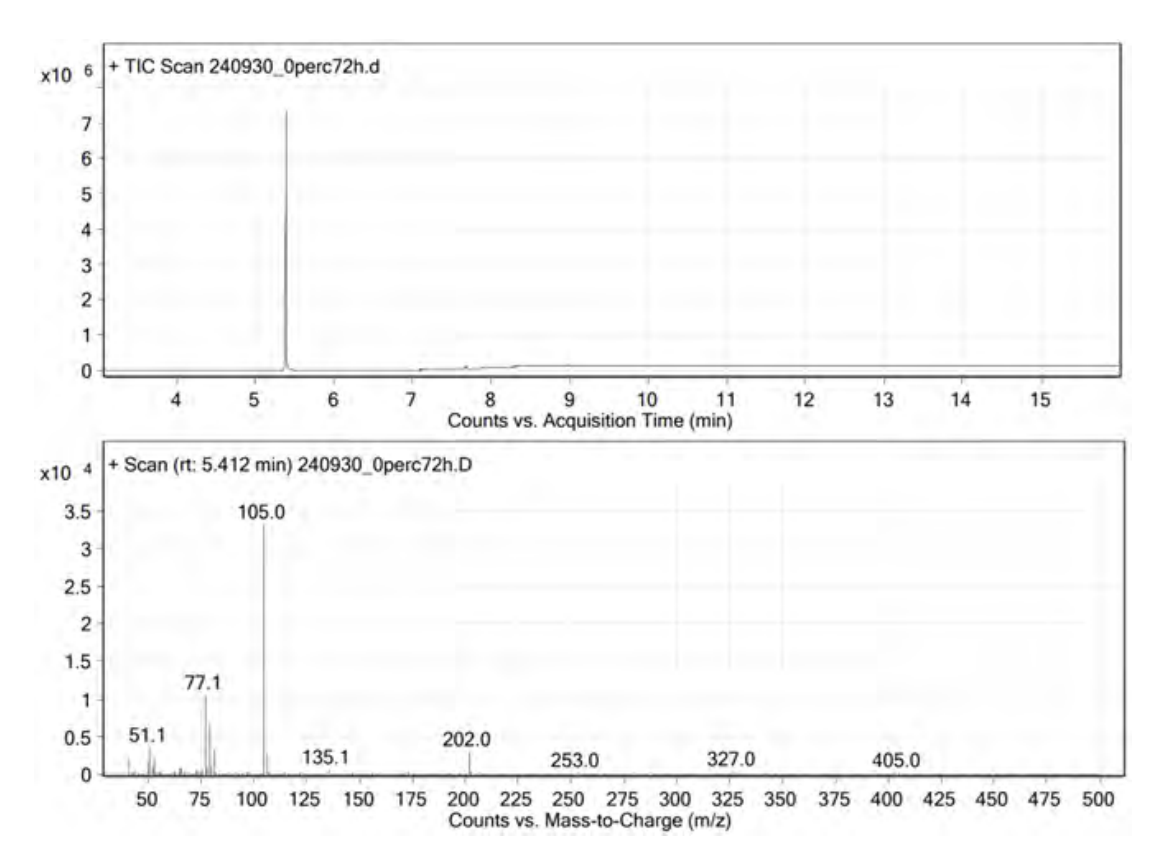


Figure A17: A GC chromatogram (top) and mass spectrum (bottom) of 0 wt% 72 h cobalt (II) stearate oxidised sample for model compound 2.

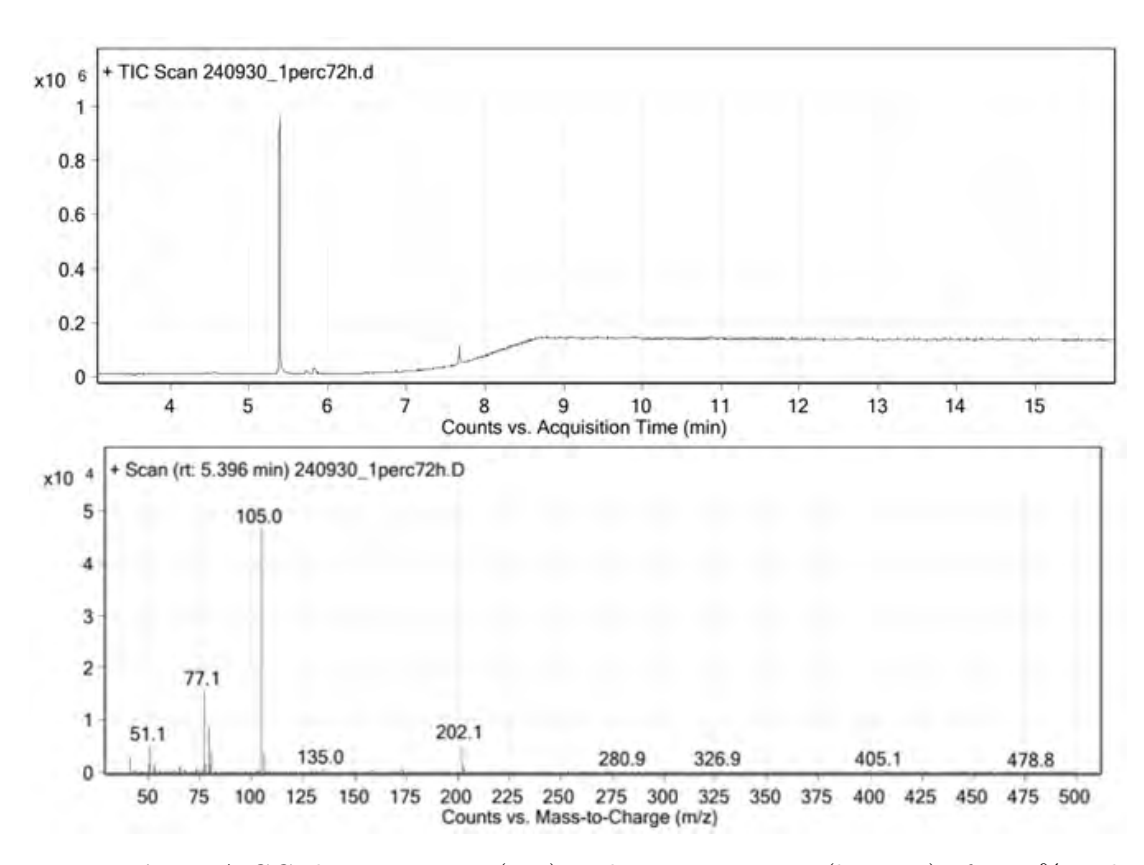


Figure A18: A GC chromatogram (top) and mass spectrum (bottom) of 1 wt% 72 h cobalt (II) stearate oxidised sample for model compound **2**.

References

- 1 Editorial Board. "The future of plastic". Nat. Commun. 9 (2018). Editorial, p. 2157.
- 2 I. Slav. How Much Crude Oil Does Plastic Production Really Consume? https://oilprice.com/Energy/Energy-General/How-Much-Crude-Oil-Does-Plastic-Production-Really-Consume.html (Accessed April 2025).
- 3 Statista. Annual production of plastics worldwide from 1950 to 2023. 2025. https://www.statista.com/statistics/282732/global-production-of-plastics-since-1950/ (Accessed April 2025).
- 4 Plastics Europe. Food Waste. https://plasticseurope.org/sustainability/circularity/waste-management-prevention/food-waste/ (Accessed April 2025).
- 5 CuSP. How much plastic is recycled? 2024. https://www.cuspuk.com/news/how-much-plastic-is-recycled/ (Accessed April 2025).
- 6 Waste Managed. Glass vs Plastic Packaging What's Better? https://www.wastemanaged.co.uk/our-news/glass-waste/glass-vs-plastic-packaging-whats-better/ (Accessed April 2025).
- 7 Plastics Europe. *Mobility and transport*. https://plasticseurope.org/sustainability/sustainable-use/sustainable-mobility-transport/ (Accessed April 2025).
- 8 R. Tiwari et al. "A critical review and future perspective of plastic waste recycling". Sci. Tot. Env. 881.7 (2023), p. 163433.
- 9 G. Casillas et al. "Microplastics Scoping Review of Environmental and Human Exposure Data". *Microplastics* 2.1 (2023), pp. 78–92.

- 10 L. Lebreton et al. "Evidence that the Great Pacific Garbage Patch is rapidly accumulating plastic". *Nature* 8 (2018), p. 4666.
- 11 United Nations. Transforming Our World: The 2030 Agenda for Sustainable Development (A/RES/70/1). United Nations, 2015. https://sdgs.un.org/2030agenda (Accessed September 2025).
- 12 S. M. Vega Gutierrez et al. "Wood Cutting Board Finishes and Their Effect on Bacterial Growth". *Coatings* 13.4 (2023), p. 752.
- 13 R. Geyer, J. R. Jambeck, and K. L. Law. "Production, use, and fate of all plastics ever made". Sci. Adv. 3 (2017), e1700782.
- 14 Statista. Production capacity of polyethylene terephthalate worldwide from 2014 to 2024. 2020. https://www.statista.com/statistics/242764/global-polyethylene-terephthalate-production-capacity/ (Accessed April 2025).
- 15 T. M. Joseph et al. "Polyethylene terephthalate (PET) recycling: A review". Case Studies in Chemical and Environmental Engineering 9 (2024), p. 100673.
- 16 Ecochain. What has the lowest impact: glass vs. plastic packaging. 2025. https://ecochain.com/customers/case-study-packaging-plastic-vs-glass/(Accessed April 2025).
- 17 S. Chairat and S. H. Gheewala. "Life cycle assessment and circularity of polyethylene terephthalate bottles via closed and open loop recycling". *Environ. Res.* 236.Part 1 (2023), p. 116788.
- 18 SaveMoneyCutCarbon. How long does it take for plastic to biodegrade? https://www.savemoneycutcarbon.com/learn-save/how-long-does-it-take-for-plastic-to-biodegrade/ (Accessed April 2025).

- 19 M. T. Hossain et al. "Techniques, applications, and prospects of recycled polyethylene terephthalate bottle: A review". *J. Thermoplast. Compos. Mater.* 37.3 (), pp. 1268–1286.
- 20 M. Hughes. How long it takes everyday items to decompose. 2022. https://www.forgerecycling.co.uk/blog/how-long-it-takes-everyday-items-to-decompose/ (Accessed April 2025).
- 21 T. S. Gomes, L. L. Y. Visconte, and E. B. A. V. Pacheco. "Life Cycle Assessment of Polyethylene Terephthalate Packaging: An Overview". J. Polym. Environ. 27 (2019), pp. 533–548.
- 22 T. Li et al. "A system boundary identification method for life cycle assessment". *Int. J. Life Cycle Assess.* 19 (2013), pp. 646–660.
- 23 Y. Saleh. "Comparative life cycle assessment of beverages packages in Palestine". J. Clean. Prod. 131 (2016), pp. 28–42.
- 24 C. Detrois and T. Steinbauer. *Bottles, preforms and closures: a design guide* for pet packaging. 2nd. New York, U.S.A.: Elsevier Inc., 2012.
- 25 C.-E. Komly et al. "Multiobjective waste management optimization strategy coupling life cycle assessment and genetic algorithms: Application to PET bottles". Resour. Conserv. Recycl. 69 (2012), pp. 66–81.
- 26 M. Hyvärinen, M. Ronkanen, and T. Kärki. "Sorting efficiency in mechanical sorting of construction and demolition waste". *Waste Manag. Res.* 38.7 (2020), pp. 812–816.
- 27 S. R. Ahmad. "A New Technology for Automatic Identification and Sorting of Plastics for Recycling". *Environ. Technol.* 25.10 (2010), pp. 1143–1149.
- 28 Aloxe Holding B.V. Our Technology: Mechanical Recycling. (Accessed April 2025). https://www.aloxe.one/mechanical-recycling.html.

- 29 C. D. B. Fernández et al. "Microbial degradation of polyethylene terephthalate: a systematic review". SN Appl. Sci. 4 (2022), p. 263.
- 30 Coperion. *PET Recycling Bottle-to-Fiber*. https://coperion.com/en/industries/plastics-recycling/pet-recycling-bottle-to-fiber (Accessed April 2025).
- 31 P. Benyathiar et al. "Polyethylene Terephthalate (PET) Bottle-to-Bottle Recycling for the Beverage Industry: A Review". *Polymers* 14.12 (2022), p. 23.
- 32 CEFIC. Recycling more plastics: PET packaging. https://cefic.org/a-solution-provider-for-sustainability/chemistrycan/driving-the-circular-economy/recycling-more-plastics/ (Accessed April 2025).
- 33 E. Pinter et al. "Circularity Study on PET Bottle-To-Bottle Recycling". Sustainability 13.13 (2021), p. 7370.
- 34 M. T. Brouwer, F. Alvarado Chacon, and E. U. Thoden van Velzen. "Effect of recycled content and rPET quality on the properties of PET bottles, part III: Modelling of repetitive recycling". 33.9 (2020), pp. 373–383.
- 35 Zero Waste Europe. New report: PET, the most circular of all plastics, is far from real circularity. 2022. https://zerowasteeurope.eu/press-release/new-report-pet-the-most-circular-of-all-plastics/ (Accessed April 2025).
- 36 M. A. Suarez et al. "Selective H_2 production from plastic waste through pyrolysis and in-line oxidative steam reforming". *Energy* 302 (2024), p. 131762.
- 37 B. Kunwar et al. "Plastics to fuel: a review". Renewable and Sustainable Energy Reviews 54.C (2016), pp. 421–428.
- 38 Royal Society of Chemistry. *Chemical recycling*. https://www.rsc.org/globalassets/22-new-perspectives/sustainability/progressive-plastics/explainers/rsc-explainer-6---chemical-recycling.pdf (Accessed April 2025).

- 39 J. Jiang et al. "From plastic waste to wealth using chemical recycling: A review". J. Environ. Chem. Eng. 10.1 (2022), p. 106867.
- 40 Z. Stein. *Gasification*. 2024. https://www.carboncollective.co/sustainable-investing/gasification (Accessed April 2025).
- 41 A. Lamtai et al. "Mechanical Recycling of Thermoplastics: A Review of Key Issues". Waste 1.4 (2023), pp. 860–883.
- 42 British Plastics Foundation. *Chemical Recycling 101*. https://www.bpf.co.uk/plastipedia/chemical-recycling-101.aspx (Accessed April 2025).
- 43 Royal Society of Chemistry. *Mechanical recycling*. https://www.rsc.org/globalassets/22-new-perspectives/sustainability/progressive-plastics/explainers/rsc-explainer-5---mechanical-recycling.pdf (Accessed April 2025).
- 44 K. Tumu, K. Vorst, and G. Curtzwiler. "Understanding intentionally and non-intentionally added substances and associated threshold of toxicological concern in post-consumer polyolefin for use as food packaging materials". 10.1 (2024), e23620.
- 45 "What a waste! Evidence of consumer food waste prevention and its effectiveness". Sustain. Prod. Consum. 41 (2023), pp. 305–319.
- 46 V. Amicarelli and C. Bux. "Food waste measurement toward a fair, healthy and environmental-friendly food system: a critical review". *Br. Food J.* 123.8 (2021), pp. 2907–2935.
- 47 United Nations. Wasting food just feeds climate change, new UN environment report warns. 2021. https://news.un.org/en/story/2021/03/1086402 (Accessed April 2025).
- 48 Food and Agriculture Organization of the United Nations. Food Loss and Food Waste. 2021. https://www.fao.org/policy-support/policy-themes/food-

- loss-and-food-waste/-Food-Loss-and-Food-Waste-Database/en (Accessed April 2025).
- 49 M. Rezaei and B. Liu. Food loss and waste in the food supply chain. 2017. https://openknowledge.fao.org/server/api/core/bitstreams/36cb45bc-392c-41fb-97f1-90ca1f16ee7f/content (Accessed April 2025).
- 50 V. Siracusa et al. "Biodegradable polymers for food packaging: a review". Trends Food Sci. Technol. 19.12 (2008), pp. 634–643.
- 51 M. M. Abd Al-Ghani, R. A. Azzam, and T. M. Madkour. "Design and Development of Enhanced Antimicrobial Breathable Biodegradable Polymeric Films for Food Packaging Applications". *Polymers* 13.20 (2021), p. 3527.
- 52 S. Shaikh, M. Yaqoob, and P. Aggarwal. "An overview of biodegradable packaging in food industry". Curr. Res. Food Sci. 4 (2021), pp. 503–520.
- 53 M. S. Vakkalanka et al. "7 Emerging packaging technologies for fresh produce". Emerging Food Packaging Technologies: Principles and Practice. Ed. by K. L. Yam and D. S. Lee. Cambridge, England, United Kingdom: Woodhead Publishing Limited, 2012, pp. 109–133.
- 54 L. Vermeiren et al. "Developments in the active packaging of foods". *Trends Food Sci. Technol.* 10.3 (1999), pp. 77–86.
- 55 M. W. Ahmed et al. "A review on active packaging for quality and safety of foods: Current trends, applications, prospects and challenges". Food Packag. Shelf Life 33 (2022), p. 100913.
- 56 C. S. Barry and J. J. Giovannoni. "Ethylene and Fruit Ripening". *J. Plant Growth Regul.* 26 (2007), pp. 143–159.
- 57 Z. Asim et al. "Significance of Sustainable Packaging: A Case-Study from a Supply Chain Perspective". Appl. Syst. Innov. 5.6 (2022), p. 117.

- 58 S. A. Cichello. "Oxygen absorbers in food preservation: a review". *J. Food Sci. Technol.* 52 (2015), pp. 1889–1895.
- 59 N. J. Astrini et al. "Identifying objective quality attributes of functional foods". Qual. Assur. Saf. Crops Foods 12.2 (2020), pp. 24–39.
- 60 A. G. Azevedo et al. "Active Flexible Films for Food Packaging: A Review". *Polymers* 14.12 (2022), p. 2442.
- 61 E. Kütahneci and Z. Ayhan. "Applications of different oxygen scavenging systems as an active packaging to improve freshness and shelf life of sliced bread". J. Consum. Prot. Food Saf. (2021), pp. 247–259.
- 62 K. K., S. S. Gaikwad, and Y. S. Lee. "Oxygen scavenging films in food packaging". *Environ. Chem. Lett.* 16 (2018), pp. 523–528.
- 63 Simple Family Preparedness. How to Use Oxygen Absorbers For Food: A Step By Step Guide. https://simplefamilypreparedness.com/how-to-use-oxygen-absorbers/ (Accessed February 2025).
- 64 K. K. Gaikwad, S. Singh, and Y. S. Lee. "Oxygen scavenging films in food packaging". *Environ. Chem. Lett.* 16 (2018), pp. 523–538.
- 65 M. Ozdemir and J. D. Floros. "Active Food Packaging Technologies". Crit. Rev. Food Sci. Nutr. 44.3 (2004), pp. 185–193.
- 66 M. Ozdemir and J. D. Floros. "Active Food Packaging Technologies". Critical Reviews in Food Science and Nutrition 44.3 (2004), pp. 185–193. https://www.tandfonline.com.
- 67 Mitsubishi Gas Chemical. Outline of Nylon-MXD6. https://www.mgc.co.jp/eng/products/ac/nmxd6/about.html#:~:text=Nylon%2DMXD6%20is%20a%20generic,of%20MXDA%20with%20adipic%20acid (Accessed April 2025).

- 68 P. J. Cahill and S. Y. Chen. "Oxygen scavenging condensation copolymers for bottles and packaging articles". US6083585A (U.S.). C. H. Inc. 1996.
- 69 A. N. Pilipenko, B. T. Sharipov, and F. A. Valeev. "Eleuthesides and their analogs: VII. Synthesis of menthane derivatives by the Diels-Alder reaction of levoglucosenone with (2E,4E)-hexa-2,4-dien-1-yl acetate". Russ. J. Org. Chem. 50 (2014), pp. 1504–1510.
- 70 M. Kotova et al. "Selective hydrogenation of C6 dienic compounds using homogeneous Cp*-ruthenium (II) catalyst". React. Kinet., Mech. Catal. 125 (2018), pp. 619–631.
- 71 M. J. Ball. "Oxidation studies of a novel barrier polymer system". PhD thesis.

 The University of Aston in Birmingham, 1995.
- 72 M. O. Lederer. "Reactivity of Lysine Moieties toward -Hydroxy-, -unsaturated Epoxides: A Model Study on Protein—Lipid Oxidation Product Interaction". J. Agric. Food Chem. 44 (1996), 2531—2537.
- 73 University College London. Spin-lattice and spin-spin relaxation. https://www.ucl.ac.uk/nmr/sites/nmr/files/L5_3SH_web_shortened.pdf (Accessed April 2025).
- 74 LibreTexts Chemistry. 5.3: Factors That Influence NMR Chemical Shift. https://chem.libretexts.org/Courses/Providence_College/Organic_Chemistry_I/05%3A_Analytical_Methods_for_Structure_Elucidation/5. 03%3A_Factors_That_Influence_NMR_Chemical_Shift (Accessed April 2025).
- 75 P. Gijsman. "Review on the thermo-oxidative degradation of polymers during processing and in service". e-Polymers 8.1 (2008), p. 65.

76 ISH via Agilent Answers. Siloxane Peaks in Total Ion Chromatogram (TIC). 2016. https://community.agilent.com/technical/gcms/m/files/602 (Accessed April 2025).